J. Fluid Mech. (2020), *vol*. 904, A6. © The Author(s), 2020.
Published by Cambridge University Press
doi:10.1017/jfm.2020.662

Lift and drag forces acting on a particle moving with zero slip in a linear shear flow near a wall

Nilanka I. K. Ekanayake[1], Joseph D. Berry[1], Anthony D. Stickland[1], David E. Dunstan[1], Ineke L. Muir[2], Steven K. Dower[2] and Dalton J. E. Harvie[1],†

[1]Department of Chemical Engineering, The University of Melbourne, Victoria 3010, Australia

[2]Bio21 Molecular Science and Biotechnology Institute, CSL, Victoria 3052, Australia

(Received 11 February 2020; revised 15 June 2020; accepted 30 July 2020)

The lift and drag forces acting on a small spherical particle in a single wall-bounded linear shear flow are examined via numerical computation. The effects of shear rate are isolated from those of slip by setting the particle velocity equal to the local fluid velocity (zero slip), and examining the resulting hydrodynamic forces as a function of separation distance. In contrast to much of the previous numerical literature, low shear Reynolds numbers are considered ($10^{-3} \lesssim Re_\gamma \lesssim 10^{-1}$). This shear rate range is relevant when dealing with particulate flows within small channels, for example particle migration in microfluidic devices being used or developed for the biotech industry. We demonstrate a strong dependence of both the lift and drag forces on shear rate. Building on previous theoretical $Re_\gamma \ll 1$ studies, a wall-shear-based zero-slip lift correlation is proposed that is applicable when the wall lies both within the inner and outer regions of the disturbed flow. Similarly, we validate an improved wall-shear-based zero-slip drag correlation that more accurately captures the drag force when the particle is close to, but not touching, the wall. Application of the new correlations to predict the movement of a force-free particle shows that the examined shear-based lift force is as important as the previously examined slip-based lift force, highlighting the need to accurately account for shear when predicting the near-wall movement of force-free particles.

Key words: particle/fluid flow, microfluidics, suspensions

1. Introduction

Particles moving in a sheared flow exhibit cross-stream migration and cluster at different equilibrium distances across channels (Segre & Silberberg 1962). In the absence of inter-particle collisions (i.e. a dilute suspension), this clustering is primarily a result of hydrodynamic lift forces that cause particles to migrate in a direction normal to the flow. Lift forces can be important in (for example) cancer-detecting and cell-sorting applications used in novel microfluidic devices and for flow cytometry (Di Carlo *et al.* 2009). In the context of blood flow, lift forces may aid in the separation of platelets from red blood cells, causing the formation of a cell-free layer (CFL) adjacent to blood vessel walls. CFL development is crucial for blood clot formation, as the platelet concentration is increased in

† Email address for correspondence: daltonh@unimelb.edu.au

the CFL, enhancing the haemostatic coagulation mechanisms required to repair damaged vessel walls (Leiderman & Fogelson 2011).

Hydrodynamic lift forces are inertial in origin, and hence reduce to zero for rigid particles in the Stokes (low Reynolds number) limit (Bretherton 1962). At finite Reynolds numbers and in unbounded linear flows, rigid particles experience lift when moving relative to the undisturbed fluid velocity (i.e. at a finite slip velocity) either when there is finite shear within the fluid, or particle rotation relative to the fluid (Rubinow & Keller 1961; Saffman 1965). In bounded flows (i.e. near a wall), particles moving at finite Reynolds numbers experience an additional lift force even in the absence of slip. Additionally, the drag force, which is often much higher in magnitude than the lift force, is also affected by the presence of a wall, causing neutrally buoyant particles moving at small but finite Reynolds numbers tangential to a wall to lag the fluid (Goldman, Cox & Brenner 1967*b*). Few studies have analysed the lift and drag forces acting on a particle due to shear and/or rotation near a wall when there is no particle slip, however, knowledge of these forces is required to model the cross-stream migration of neutrally buoyant particles, relevant to applications including those described above. Hence the motivation for this study.

The lift force acting on a rigid sphere was first examined by Saffman (1965), who considered a buoyant particle moving at a finite slip velocity in an unbounded linear shear flow. The model considered the inertial effects of the far field disturbed flow on the lift force, at low slip and shear Reynolds numbers ($Re_{slip} \ll 1$, $Re_\gamma \ll 1$), where

$$Re_{slip} = \frac{|u_{slip}|a}{\nu}, \quad Re_\gamma = \frac{|\gamma|a^2}{\nu}, \tag{1.1a,b}$$

and u_{slip}, a, ν and γ are the particle slip velocity, particle radius, fluid kinematic viscosity and fluid shear rate, respectively. These Reynolds numbers are defined based on slip and shear magnitudes. Unlike shear-free flows, in which the Stokes length scale ($L_S = \nu/|u_{slip}|$) is used to separate the inner and outer regions, an additional length scale known as the Saffman length scale ($L_G = \sqrt{\nu/|\gamma|}$) is considered for linear shear flows. Generally, the boundary of the inner and outer regions in a linear shear flow field is located at $\min(L_G, L_S)$. Saffman's lift is an 'outer region' model that solves the velocity field in the region far away from the particle where both viscous and inertial effects are significant. Specifically, an Oseen-type equation is solved via a matched asymptotic expansion method and the flow disturbance due to the particle is determined by treating the particle as a point force. This model neglects the significance of viscous effects in the 'inner region' closer to the particle. In addition to the low Reynolds number condition, Saffman's lift model is valid only when the inertial effects due to shear rate are much higher than the inertial effects generated by slip velocity ($\epsilon = \sqrt{|Re_\gamma|}/Re_{slip} \gg 1$ or equivalently $L_G \ll L_S$). Asmolov (1990) and McLaughlin (1991) independently relaxed this constraint on ϵ by presenting an unbounded lift model for comparable inertial effects ($\sqrt{|Re_\gamma|} \sim Re_{slip}$) that reduces to Saffman's result when $\epsilon \to \infty$. The above unbounded lift models reduce to zero if either Re_{slip} or Re_γ is zero.

Particle rotation also affects the forces experienced by a particle. A force-free particle in an unbounded shear flow rotates at a rate corresponding to a zero torque condition and hence, experiences a rotational lift force (Rubinow & Keller 1961). However, in a linear shear flow, Saffman (1965) illustrated that the lift force due to rotation is less by an order of magnitude than that due to the slip-shear of a freely rotating sphere translating with a small slip. Thus, most unbounded lift models only consider a non-rotating particle (Asmolov 1990; McLaughlin 1991).

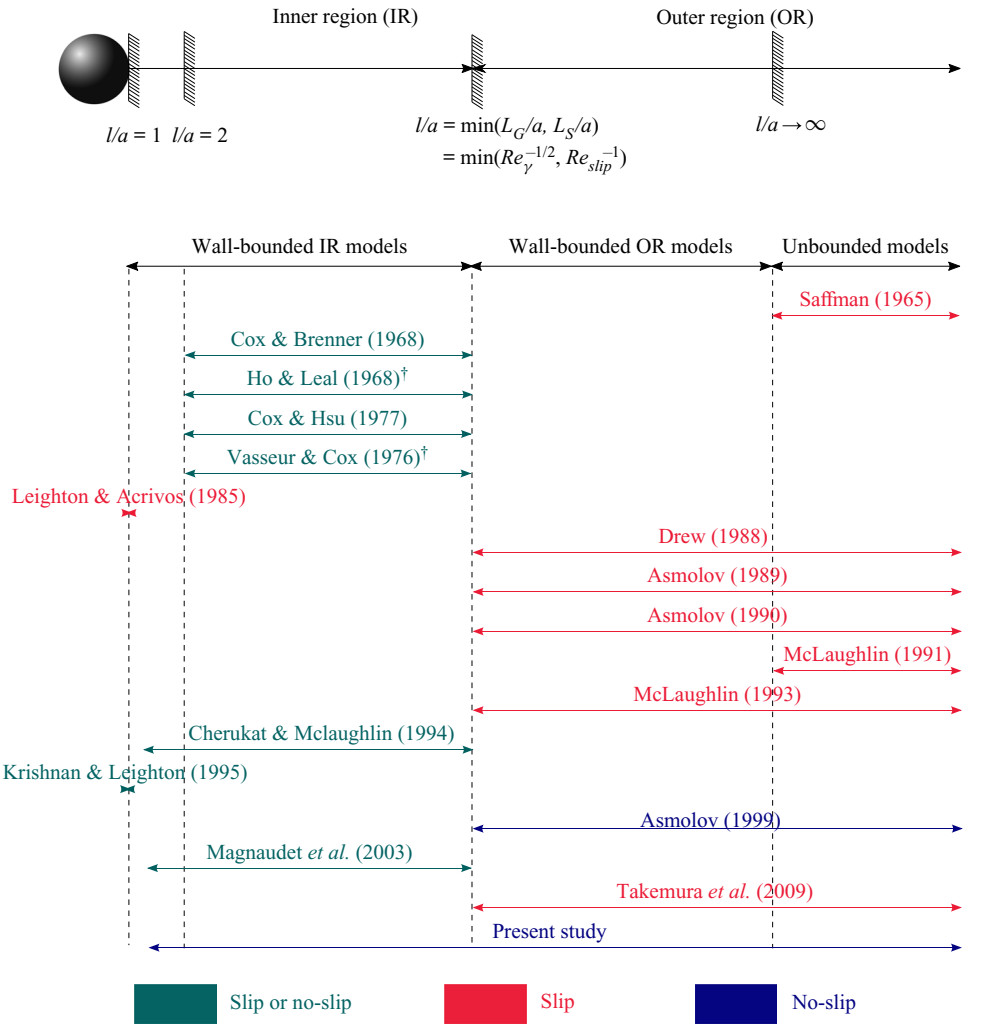

FIGURE 1. Analytical lift force models available for linear shear flows illustrating the range of applicability based on dimensionless wall distance (l/a) and on 'slip' and 'no-slip' conditions. The lift coefficient of 'slip' models scales with Re_{slip} and Re_γ whereas the lift coefficient of 'no-slip' models scales only with Re_γ. †Models bounded by two walls.

In addition to the slip-shear and rotation effects, the presence of a wall near a particle also affects the hydrodynamic forces experienced by that particle. These wall-induced inertial forces have been discussed in a number of 'bounded flow' studies. Figure 1 summarises the available analytical lift models for both these bounded and unbounded flows. As illustrated, in bounded flow models the walls can reside in either the inner or outer regions of the disturbed flow surrounding the particle.

Most theoretical wall-bounded lift models require the wall to lie within the inner region, $l \ll \min(L_G, L_S)$, where l is the distance between the particle centre and the wall. Additionally, these models require $Re_{slip}, Re_\gamma \ll 1$. Inner region models are applicable for particles with either zero or finite slip velocities. Most early inner region studies use the term 'neutrally buoyant' to refer to particles moving with zero slip and 'buoyant' to refer

to particles moving with a finite slip. However, in reality, neutrally buoyant particles in a linear shear flow experience a finite slip very close to a wall ($l/a \sim 1$), caused by the wall-shear-induced drag acting on the particle (a subject of the present study). Hence, the terms 'neutrally buoyant' and 'zero slip' (or 'buoyant' and 'finite slip') are not strictly equivalent. Nevertheless, for the conditions considered in these early inner region studies, the slip decays rapidly to zero as the distance between the particle and the wall increases (Goldman *et al.* 1967*b*). Given that these early models are deduced for the condition $l/a \gg 1$, their interchangeable use of the terms 'zero slip' and 'neutrally buoyant' is justified. More generally, however, a neutrally buoyant particle is not necessarily moving at precisely the fluid velocity, and the terms 'zero slip' and 'neutrally buoyant' are not equivalent. In the remainder of the study we avoid using the terms 'neutrally buoyant' and 'buoyant' to describe particle slip.

Cox & Brenner (1968) were the first to obtain an implicit expression for the forces induced on arbitrary shaped particles by a wall lying in the inner region. This model considered zero-slip and finite-slip particles. Simplifying this model, Cox & Hsu (1977) derived a closure expression for the migration velocity (u_{mig}) of rigid spherical particles in single wall-bounded flow. The equivalent lift force was also calculated using Stokes law. The model is valid only when the separation distance is large compared to the sphere radius ($l/a \gg 1$), with the equation for the force having a leading-order term proportional to l/a. Using the method of reflections, Ho & Leal (1974) explicitly calculated the lift force acting on a freely rotating, zero-slip particle bounded by two flat walls for both Couette and Poiseuille flows at low Reynolds numbers. This inner region study accounted for the effects of both walls and the flow curvature present in Poiseuille flow. For Couette flow the model predicted that particles migrate towards the channel centre due to a wall-shear lift force that is greatest near the walls but zero at the channel centre. The predicted particle migration in Couette flow agrees substantially with the experimental observations of Halow & Wills (1970). Later, Vasseur & Cox (1976) extended the theoretical work of Cox & Hsu (1977) to analyse the migration velocity of spherical particles in linear flows bounded by two flat plates, with both plates residing in the inner region of the particle. The predicted migration velocities of Vasseur & Cox (1976) for zero-slip particles agreed well with the results of Ho & Leal (1974) in the channel centre, but deviated significantly in the vicinity of the wall. As explained in Vasseur & Cox (1976), this deviation is due to poor convergence of the numerical computation in the Ho & Leal (1974) solution, particularly when the sphere is close to a wall. The same model predictions of Vasseur & Cox (1976) agreed well with the asymptotic behaviour suggested by the single wall Cox & Hsu (1977) model when the particle is near one of the walls.

Several other inner region studies (Leighton & Acrivos 1985; Cherukat & McLaughlin 1994; Krishnan & Leighton 1995) have performed lift force analyses when the particle is almost in contact with the wall ($l/a \gtrsim 1$). In contrast to other inner region studies where the particle is usually treated as a point force, these studies consider higher-order contributions to the flow disturbances induced by the particle, accounting for the finite size of the particle. The limiting case of a stationary particle touching the wall (Leighton & Acrivos 1985) and a force-free and freely rotating particle almost in contact with a wall (Krishnan & Leighton 1995) in a linear shear flow were studied using lubrication analysis to predict asymptotic lift coefficient values. Accounting for the finite size of the particle, the lift force variation with wall distance was analysed by Cherukat & McLaughlin (1994), down to a minimum separation distance of $l/a = 1.1$. The extrapolated results for a particle touching the wall agreed well with latter studies (Leighton & Acrivos 1985; Krishnan & Leighton 1995) for both fixed and force-free cases. More recently, Magnaudet,

Takagi & Legendre (2003) derived inner region solutions for a spherical bubble and a rigid particle moving freely near a wall and proposed lift correlations valid for $l/a \gtrsim 1$.

In all the inner region studies, the lift force on both freely rotating and non-rotating particles is obtained by coupling the two flow disturbances that originate from particle slip and fluid shear, the stokeslet and stresslet, respectively, in a nonlinear manner. These inner region lift models, strictly valid for $Re_{slip}, Re_\gamma \ll 1$, present the force as

$$F_L^* = \frac{F_L \rho}{\mu^2} = C_{L,1} Re_\gamma^2 + \mathrm{sgn}(\gamma^*) C_{L,2} Re_\gamma Re_{slip} + C_{L,3} Re_{slip}^2, \tag{1.2}$$

where $\gamma^* = \gamma a / u_{slip}$, and the three lift coefficients ($C_{L,1}$, $C_{L,2}$, $C_{L,3}$) are functions of a/l. A positive (negative) sign for γ^* indicates a leading (lagging) particle in a positive shear flow or a lagging (leading) particle in a negative shear flow. Here, $C_{L,1}$ is associated with the force in the absence of slip ($Re_{slip} = 0$), and the first term on the right-hand side of (1.2) originates from the disturbance induced by the presence of the wall in a shear flow field. Similarly, $C_{L,3}$ is associated with the force in the absence of shear ($Re_\gamma = 0$), and the last term in the same equation is due to the stokeslet generated from slip velocities in a quiescent fluid next to a wall. The remaining coefficient, $C_{L,2}$, captures remaining variations in the presence of both the slip and shear, particularly when slip and shear are of the same order of magnitude. Therefore the force given by the second term depends on both slip velocity and shear rate. The first and last terms in (1.2) produce forces that are directed into the fluid, resulting in positive lift. The lift force due to the second term depends on both the slip and shear rate directions, with the direction of this force captured by the sign of γ^*.

As the inner region models require a particle to be close to a wall, they cannot be used to predict unbounded results as l/a becomes large. Instead, a few authors have investigated the effect of walls lying in outer region of the disturbed flow, that is, under conditions where $Re_\gamma, Re_{slip} \ll 1$. These outer region wall-bounded models use the method of matched asymptotic expansions to solve the singular perturbation problem by treating the particle as a point force. Unlike inner region models, outer region models correctly predict the unbounded results as $l/L_G \to \infty$. Outer region studies analysing a particle sedimenting in a stagnant fluid ($Re_\gamma = 0$) have presented lift correlations as functions of l/L_S (Vasseur & Cox 1977; Takemura & Magnaudet 2003; Takemura 2004; Shi & Rzehak 2020). Similarly, linear shear flows bounded by a single wall were examined by Drew (1988) and Asmolov (1989) for the condition $\epsilon \gg 1$. Later, Asmolov (1990) and McLaughlin (1993) extended their previous analysis to single wall-bounded linear flows valid for all ϵ. The latter two studies considered a non-rotating, buoyant spherical particle with a finite slip velocity and the calculated lift coefficients were tabulated/plotted as a function of l/L_G and ϵ. Using a similar approach, Asmolov (1999) evaluated the lift force coefficient for a freely rotating zero-slip particle in a linear shear flow bounded by a single wall located in the outer region. Recently, Takemura, Magnaudet & Dimitrakopoulos (2009) obtained a semi-empirical lift coefficient model based on the McLaughlin results which recovers the correct asymptotic behaviours when the particle is located both near and far from the wall, for $\epsilon \gg 1$ and $\epsilon \ll 1$ conditions. However, as this correlation only captures slip-shear-based lift, it predicts zero lift for a zero-slip particle.

In this study we are particularly interested in the lift force on a zero-slip particle. When the wall is located close to the particle (in the inner region of the disturbed flow field), the lift force can be evaluated from (1.2) by using $Re_{slip} = 0$. Noting that F_L is non-dimensionalised by $\rho a^4 \gamma^2 (= {Re_\gamma}^2 \mu^2 / \rho)$, we see that the net lift force is determined by the first lift coefficient ($C_{L,1}$). The available formulations for $C_{L,1}$ are summarised

https://doi.org/10.1017/jfm.2020.662 Published online by Cambridge University Press

Study	$C_{L,1}$	Comments	Equation
Cox & Hsu (1977)	$\frac{366\pi}{576}$	Non-rotating, $l/a \gg 1$	(1.3)
	$\frac{330\pi}{576}$	Freely rotating, $l/a \gg 1$	(1.4)
Cherukat & McLaughlin (1994)	$2.0069 + 1.0575\left(\frac{a}{l}\right) - 2.4007\left(\frac{a}{l}\right)^2 + 1.3174\left(\frac{a}{l}\right)^3$	Non-rotating, $l/a \gtrsim 1$	(1.5)
Cherukat & McLaughlin (1995)	$1.8065 + 0.89934\left(\frac{a}{l}\right) - 1.961\left(\frac{a}{l}\right)^2 + 1.02161\left(\frac{a}{l}\right)^3$	Freely rotating, $l/a \gtrsim 1$	(1.6)
Krishnan & Leighton (1995)	1.9680	Non-rotating, $l/a = 1$	(1.7)
	1.6988	Freely rotating, $l/a = 1$	(1.8)
Magnaudet *et al.* (2003)	$\frac{55\pi}{96}\left[1 + \frac{9}{16}\left(\frac{a}{l}\right)\right]$	Freely rotating, $l/a \gtrsim 1$	(1.9)

TABLE 1. Wall-shear lift coefficients ($C_{L,1}$) of inner region studies.

in table 1. The listed inner region models are valid only for low shear and slip Reynolds numbers ($Re_\gamma, Re_{slip} \ll 1$), with the lift coefficients ($C_{L,1}$) asymptoting to a finite value of $\sim$1.9 for a non-rotating sphere and $\sim$1.8 for a freely rotating sphere as the particle approaches the wall (Cox & Hsu 1977; Cherukat & McLaughlin 1994; Krishnan & Leighton 1995). Conversely, when l/a becomes large, although the inner region models predict a finite lift coefficient ($C_{L,1}$) with increasing separation distance (for finite but low Re_γ), as the wall moves from the inner to outer region the results become invalid. Conversely, most models that are valid when the wall resides in the outer region (Asmolov 1989, 1990; McLaughlin 1993; Takemura *et al.* 2009) predict a zero lift force for a no-slip particle as the force scales with Re_{slip} in addition to Re_γ. As an exception, Asmolov (1999) derived an outer region wall-bounded lift model for zero-slip particles that gives a lift force that scales with Re_γ and varies as a function of l/L_G. Nevertheless, no analytical model is able to predict the lift force on a zero-slip particle across both the inner and outer regions of the flow, as a function of the shear rate within the fluid.

Drag, a force present in both Stokes and inertial flows, is equally as important as the lift force in predicting the migration of particles, as drag can induce slip, and in the presence of wall slip alone (or slip plus shear) can induce a lift force. In unbounded fluid flow, drag is only a function of the slip velocity of the particle, however, the presence of a wall increases this slip-induced drag such that it is highest when the particle is in contact with the wall, and decays rapidly to the unbounded value as the separation distance increases. Analyses of wall-bounded slip-induced drag have been conducted for both Stokes (Goldman, Cox & Brenner 1967*a*; Goldman *et al.* 1967*b*; Happel & Brenner 1981; Magnaudet *et al.* 2003) and inertial flows (Vasseur & Cox 1977). For Stokes flows, Faxen (1922) and Happel & Brenner (1981) deduced a wall correction for the slip-based drag resulting in higher-order terms (in separation distance, $O((a/l)^5)$) being included in the force expansion. Using a method of matched asymptotic expansion, Vasseur & Cox (1977) suggested a slip-based inertial correction term for Faxen's inner region drag model, as well as an outer region slip-based drag model that gives the force as a function of l/L_S for zero-shear flows.

For linear shear flows, Magnaudet *et al.* (2003) presented an additional contribution to the drag force due to wall shear (independent of slip) giving the net drag force on a translating spherical particle with a wall in the inner region as

$$F_D^* = \frac{F_D \rho}{\mu^2} = -\mathrm{sgn}(\gamma) C_{D,1} Re_\gamma - \mathrm{sgn}(u_{slip}) C_{D,2} Re_{slip}. \tag{1.10}$$

Here, $C_{D,1}$, is a function of only (a/l) and $C_{D,2}$ is a function of both (a/l) and Re_{slip}. The first term in (1.10) represents the drag force due to shear (independent of slip), and is relevant for zero-slip particles in linear shear flows. Again note that (1.10) is given for a flow parallel to a flat wall. For low shear rates Magnaudet *et al.* (2003) gives $C_{D,1}$ as

$$C_{D,1} = \frac{15}{8}\pi \left(\frac{a}{l}\right)^2 \left[1 + \frac{9}{16}\left(\frac{a}{l}\right)\right]. \tag{1.11}$$

This $C_{D,1}$ reduces rapidly to zero away from the wall (Magnaudet *et al.* 2003). The second term $C_{D,2}$ in (1.10) accounts for the drag acting on the particle due to slip and asymptotes to the low Reynolds number Stokes drag value far from the wall. In comparison to the slip-based drag coefficient $C_{D,2}$, only a few studies have examined the behaviour of the inertial shear-based coefficient $C_{D,1}$. Note that a force-free ($F_D^* = 0$) particle in a linear shear flow lags the fluid flow near the wall due to the negative slip generated by the wall shear drag, as explained by Goldman *et al.* (1967*b*) under Stokes flow conditions and by Magnaudet *et al.* (2003) for finite inertial flow conditions.

In contrast to the above theoretical works, most numerical studies that calculate the forces acting on a wall-bounded particle are for intermediate Reynolds numbers $Re_\gamma, Re_{slip} \sim 0.5{-}3 \times 10^2$. Among these, simulations on translating particles performed in quiescent flows are used to evaluate the effect of separation distance on both slip-based lift and drag correlations (Zeng, Balachandar & Fischer 2005). Several other direct numerical studies examining hydrodynamic forces acting on a particle in a linear shear flow and with finite slip closer to the wall propose inertial corrections that are functions of both shear rate and slip velocity (Zeng *et al.* 2009; Lee & Balachandar 2010). To perform inner region simulations, satisfying $Re_\gamma, Re_{slip} < 1$ conditions, one must employ large computational domains with high mesh refinement near the particle surface in order to capture the small inertial forces. These simulations require high computational power. To our knowledge no numerical results have been presented for small but finite inertial conditions Re_γ or $Re_{slip} \leq O(1)$, possibly due to these computational limitations, particularly for wall-bounded flows under zero-slip conditions.

The main objective of this work is to extend the aforementioned zero-slip $Re_\gamma \ll 1$ results for the lift and drag on a particle to low but finite Reynolds numbers using results from a large number of well resolved numerical simulations. A rigid spherical particle moving at the same velocity as the fluid ($u_{slip} = 0$) in a linear shear flow tangential to a flat wall is considered. We study non-rotating as well as freely rotating spheres, for shear Reynolds numbers in the range of 10^{-3}–10^{-1}. We express our numerical results as new zero-slip lift and drag coefficient correlations, expressed as per (1.2) and (1.11) respectively, but now defined across the inner, outer and unbounded regions. In § 4, we apply the new zero-slip drag and lift correlations together with existing slip-based drag and lift correlations to analyse the motion of force-free and freely rotating particles near a wall in a linear shear flow.

2. Numerical simulations

2.1. *Problem specification*

A rigid sphere of radius a is suspended in a linear shear flow with the origin of the Cartesian coordinate system located at the centre of the sphere (figure 2*a*). The coordinate unit vectors are $\boldsymbol{e}_x$, $\boldsymbol{e}_y$ and $\boldsymbol{e}_z$. A no-slip wall is placed at distance $(0, -l, 0)$ away from sphere centre. Outer boundaries are located at large distances $L(\gg l)$ away from the sphere centre to minimise any secondary boundary effects. For this study l/a is varied from 1.2 to 9.5 to obtain the lift and drag force variation as a function of particle distance from the wall.

To obtain the forces generated due to wall and shear effects in the absence of relative motion between the particle and the fluid, the particle slip velocity $\boldsymbol{u}_{slip}$ is explicitly set to zero: That is,

$$\boldsymbol{u}_{slip} = \boldsymbol{u}_p - \boldsymbol{u}_f(\, y = 0) = \boldsymbol{0}, \tag{2.1}$$

where $\boldsymbol{u}_p = u_p \boldsymbol{e}_x$ is the particle velocity and $\boldsymbol{u}_f$ is the undisturbed fluid velocity defined as

$$\boldsymbol{u}_f = \dot{\gamma}(\, y + l)\boldsymbol{e}_x. \tag{2.2}$$

Note that under this formulation the particle is constrained to translate only in the x direction with particle velocity $u_p = \dot{\gamma} l$.

To determine the forces acting on the particle, we solve the steady-state Navier–Stokes equations in a frame of reference that moves with the particle (Batchelor 1967).

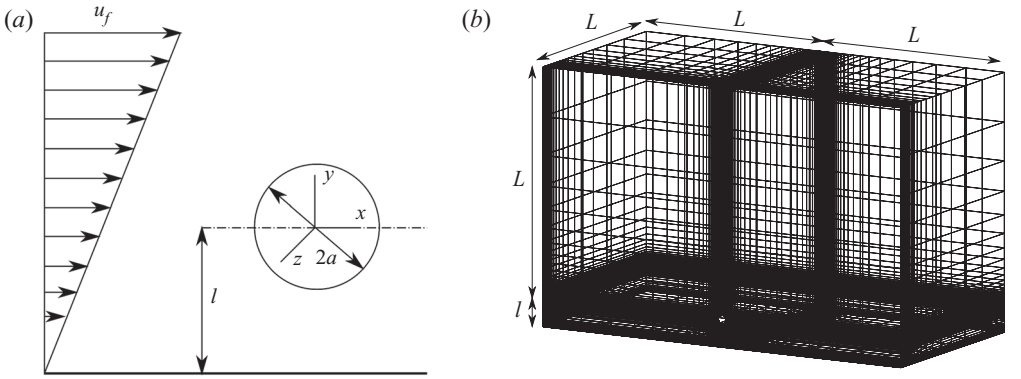

FIGURE 2. (*a*) Schematic of a translating sphere of radius a moving at velocity u_p in a wall-bounded linear shear flow. (*b*) The domain mesh for a particle located at $l/a = 4$.

Specifically, we solve

$$\nabla \cdot \rho \boldsymbol{u}' = 0, \tag{2.3}$$

$$\nabla \cdot (\rho \boldsymbol{u}'\boldsymbol{u}' + \boldsymbol{\sigma}) = 0, \tag{2.4}$$

where $\boldsymbol{u}' = \boldsymbol{u} - \boldsymbol{u}_p$ and $\boldsymbol{u}$ is the local fluid velocity. The boundary conditions used in the moving frame of reference are

$$\boldsymbol{u}' = \begin{cases} \dot{\gamma}(y + l)\boldsymbol{e}_x - \boldsymbol{u}_p, & y = +\infty;\ y = -l;\ x, z = \pm\infty, \\ \boldsymbol{\omega} \times \boldsymbol{r}, & |\boldsymbol{r}| = a, \end{cases} \tag{2.5}$$

where $\boldsymbol{r}$ is a radial displacement vector pointing from the sphere centre to the particle surface and $\boldsymbol{\omega}$ is the angular rotation of the particle.

The fluid is assumed to be Newtonian with a dynamic viscosity μ and density ρ. The total stress tensor ($\boldsymbol{\sigma} = p\boldsymbol{I} + \boldsymbol{\tau}$) (Bird, Stewart & Lightfoot (2002) sign convention), is computed using the fluid pressure, p and viscous stress tensor, $\boldsymbol{\tau} = -\mu(\nabla \boldsymbol{u}' + \nabla \boldsymbol{u}'^{\mathrm{T}})$. The forces acting on the particle are evaluated by integrating the total stress contributions around the particle surface S

$$\boldsymbol{F}_p = -\int_S \boldsymbol{n} \cdot \boldsymbol{\sigma}\, \mathrm{d}S. \tag{2.6}$$

Here, $\boldsymbol{n}(= \hat{\boldsymbol{r}})$ is a unit normal vector directed out of the particle. The drag ($F_D = \boldsymbol{F}_p \cdot \boldsymbol{e}_x$) and lift ($F_L = \boldsymbol{F}_p \cdot \boldsymbol{e}_y$) are defined as the fluid forces acting on the sphere in $+x$ and $+y$ directions, respectively. Similarly the net torque $\boldsymbol{T}_p$ acting on the particle is evaluated using

$$\boldsymbol{T}_p = -\int_S \boldsymbol{r} \times \boldsymbol{\sigma} \cdot \boldsymbol{n}\, \mathrm{d}S. \tag{2.7}$$

In this study, two cases are considered: in the first, the particle is constrained from rotating, whereas, in the second, the particle is allowed to freely rotate about the z axis, at an angular velocity ω_p. For the non-rotating (first) case all components of the rotation $\boldsymbol{\omega}$ are explicitly set to zero, whereas for the (second) freely rotating case the z component of the net torque $\boldsymbol{T}_p$ is explicitly set to zero and the z component of $\boldsymbol{\omega}$ ($\boldsymbol{\omega} \cdot \boldsymbol{e}_z = \omega_p$) is solved for as an unknown (with other components of $\boldsymbol{\omega}$ set to zero).

Unless stated otherwise, the results in the remainder of this study are presented in non-dimensional form (indicated by an asterisk) using a length scale a, velocity scale γa and force scale μ^2/ρ.

2.2. *Numerical approach*

The system of equations is solved using the finite volume package *arb* (Harvie 2010) over a non-uniform body-fitted structured mesh that is generated with *gmsh* (Geuzaine & Remacle 2009) (figure 2*b*). The sphere surface is resolved with N_p mesh points on each curved side length of a cubed sphere. This results in $6(N_p-1)^2$ cells on the sphere surface; An (N_p-1) number of inflation layers with an α geometric progression ratio around the sphere are used to capture gradients in velocity occurring near the particle wall. Outer boundaries, except the bottom wall located at $y^*=-l^*$, are placed at a distance L^* from the sphere centre in all directions. To resolve the far field of the domain (excluding the inflation layers), N_d points are used with a geometric progression β expanding towards the domain boundaries. For larger separation distances, $l^*>1.2$, (N_w-1) layers are introduced in the gap between the bounding box and the bottom wall, with a non-uniform progression of β producing more refinement near the sphere and the bottom wall. The total cell count in the mesh is N_t.

The non-dimensional lift force magnitudes measured in this study are significantly low, $|F_L^*|\sim 10^{-6}-10^{-1}$, and hence require a high resolution mesh around the sphere to accurately determine the lift coefficient. Further, the lift force is highly sensitive to the cell distribution around the particle, requiring perfect symmetry of the mesh in the y direction to correctly ensure that the lift reduces to zero as inertial effects are reduced. For this reason the symmetry of the sphere surface mesh and its surrounding cells in the bounding box are enforced by employing a 'Lego'-type construction (figure 9 in the appendix) whereby groups of mesh 'blocks' are copied, translated, rotated and joined to construct the full computational domain. For example, a single block mesh ($B1$) is copied and then rotated about the $x=0$ and $y=0$ axes to create identically discretised blocks that surround the sphere ($B1_x$, $B1_y$ and $B1_{xy}$). Similarly, the upper and lower mesh domain blocks are built using two separate block mesh entities, $B2$ and $B3$ as illustrated in figure 9, which are later rotated about $x=0$ axis. This mesh configuration ensures that we compute the zero lift force on a slip free particle under Stokes conditions down to $F_L^*\sim 10^{-15}$. The shear and slip Reynolds numbers considered in this study are sufficiently small to assume flow symmetry about the $z=0$ plane. Hence a final domain size of $[-L, L]$, $[L, -l]$ and $[L, 0]$ is used for simulations.

2.2.1. *Domain size dependency*

The domain size is first tested to determine a suitable choice of L^* such that the lift and drag forces are negligibly affected by this parameter. We perform a series of simulations where L^* is increased from 20 to 100. Simulations are performed for seven selected shear Reynolds numbers; $Re_\gamma=(1, 2, 4, 6, 8)\times 10^{-3}$, 10^{-2} and 10^{-1}; and five selected wall distances; $l^*=1.2$, 2, 4, 6 and 9.5; at $Re_{slip}=0$. The number of mesh points in the domain (N_d) is systematically increased with L^* while maintaining a constant progression ratio (β) and a constant minimum cell thickness in the outer domain.

Results for the lift and drag coefficients, $C_{L,1}$ and $C_{D,1}$ (formerly defined in § 3.1) respectively, for the minimum and maximum separation distances ($l^*=1.2$ and 9.5, respectively) and minimum and maximum shear Reynolds numbers ($Re_\gamma=10^{-3}$ and 10^{-1}) are shown in table 2. Also shown are the percentage differences (δ) for these

coefficients relative to the corresponding values obtained using the maximum domain size (L^*). We use δ as an indicator of the coefficient accuracy, noting the limitations of this measure as we approach the maximum domain size.

For $Re_\gamma \geq 10^{-2}$, a domain size of $L^* = 50$ is sufficient to capture all the inertial effects responsible for the lift forces, with δ less than 1 % for all separation distances ($1.2 \leq l^* \leq 9.5$) under both non-rotating and freely rotating conditions (additional supporting data not shown). In contrast, for low shear Reynolds numbers, for example the conditions of $Re_\gamma = 10^{-3}$, non-rotating (freely rotating) particles and a domain size of $L^* = 50$, an increase of δ from ∼0.96 % (0.64 %) to ∼12 % (9.15 %) is observed as the separation distance increases from $l^* = 1.2$ to 9.5. For smaller separation distances (i.e. $l^* = 1.2$), even at low Re_γ, smaller values for δ are expected as wall effects dominate outer boundary effects in this near-to-wall regime (Ekanayake *et al.* 2018). However, when the distance to the wall is large and Re_γ low, the lift force is quite sensitive to the location of the outer boundary. Noting that the boundary layer thickness around a translating sphere in an unbounded environment is inversely proportional to $\sqrt{Re_{slip}}$ (Dandy & Dwyer 1990), it follows that larger domain sizes are required to minimise outer boundary effects when Re_γ is small (Dandy & Dwyer 1990). Therefore, for the simulations where $Re_\gamma < 10^{-2}$, a larger domain size of $L^* = 100$ is used in this study, compared to the domain size of $L^* = 50$ used for the higher Re_γ situations. Using this strategy we believe the accuracy of all presented lift coefficients to be better than 1 %, with the possible exception of values calculated using the combination of the lowest Re_γ and highest l^* values considered.

For drag, the accuracy of the drag coefficient calculation is largely a function of wall separation distance. With the selected domain size of $L^* = 50$ that is used for the $Re_\gamma \geq 10^{-2}$ results, $\delta < 1$ % only for $l^* \leq 4$ (additional data not shown). Further away from the wall, a notable dependency on domain size is found, with a δ variation of ∼5 % (2 %) to 24 % (12 %) for non-rotating (freely rotating) conditions as l^* increases from 6 to 9.5 for $Re_\gamma = 10^{-1}$. Results for $Re_\gamma = 10^{-3}$ are similar. Also at these larger separation distances, specifically at $l^* = 8$ and 9.5, small positive drag coefficients are observed for $-C_{D,1}$ when $Re_\gamma = 10^{-1}$ (noting that results for $l^* = 4, 6, 8$ are not presented in the table). The small positive drag coefficients and larger δ values found at large separation distances are caused by small errors in $F^*_{D,1}$ which are amplified when expressed as a relative drag coefficient error, because as the separation distance increases, both the coefficients and the force approach zero. Note, however, that while the drag coefficient errors are higher at the largest separation distances, an 11 % change in domain size from $L^* = 90$ to 100 results in less than a 1 % change in drag coefficient (for $Re_\gamma = 10^{-3}$), suggesting that the results are close to independent of domain size. In summary, while the errors in the calculated drag coefficients are larger than for lift, the largest errors occur under conditions in which the drag force is low. Under conditions in which the drag force is appreciable, the error in the drag force coefficient is similar to that reported for the lift force coefficient.

2.2.2. *Mesh dependency*

The effect of mesh resolution within the boundary layers surrounding the sphere is examined in this section. The number of inflation layers around the sphere and the number of cells on the sphere surface were adjusted by varying N_p while maintaining the same progression rate α in the bounding box. Concurrently, N_d was also changed, maintaining $N_d = N_p$ for all cases.

Figure 3 shows the resulting lift coefficients and non-dimensionalised lift forces for four mesh refinement levels around the sphere and for the conditions of $l^* = 1.2$, a domain size of $L^* = 50$ and a range of shear Reynolds numbers. As $F^*_{L,1}$ reduces to zero, $C_{L,1}$

https://doi.org/10.1017/jfm.2020.662 Published online by Cambridge University Press

		Domain		Non-rotating				Freely rotating			
				Lift		Drag		Lift		Drag	
l^*	Re_γ	L^*	N_t	$C_{L,1}$	$\delta\%$	$-C_{D,1}$	$\delta\%$	$C_{L,1}$	$\delta\%$	$-C_{D,1}$	$\delta\%$
1.2	0.001	20	124 672	1.8644	6.46	−8.4178	0.54	1.7101	4.33	−7.9135	0.35
		40	149 710	1.9597	1.68	−8.4576	0.07	1.7674	1.12	−7.9373	0.05
		50	158 976	1.9740	0.96	−8.4608	0.04	1.7759	0.64	−7.9392	0.02
		80	178 960	1.9901	0.16	−8.4634	0.00	1.7866	0.11	−7.9407	0.00
		100	189 702	1.9933	—	−8.4638	—	1.7874	—	−7.9409	—
	0.1	20	124 672	1.6215	0.23	−8.3313	0.36	1.5453	0.16	−7.8553	0.22
		40	149 710	1.6188	0.06	−8.3570	0.05	1.5435	0.04	−7.8703	0.03
		50	158 976	1.6183	0.04	−8.3591	0.03	1.5432	0.02	−7.8715	0.02
		80	178 960	1.6179	0.01	−8.3610	0.00	1.5429	0.00	−7.8726	0.00
		100	189 702	1.6178	—	−8.3614	—	1.5429	—	−7.8728	—
9.5	0.001	20	186 112	0.8483	55.99	−0.0223	66.42	0.8752	50.86	−0.0396	41.27
		40	223 210	1.5593	19.12	−0.0513	22.74	1.5107	15.18	−0.0580	14.02
		50	236 736	1.6964	12.00	−0.0577	13.15	1.6180	9.15	−0.0620	8.08
		80	265 600	1.8814	2.41	−0.0649	2.27	1.7503	1.73	−0.0665	1.39
		90	265 600	1.9091	0.97	−0.0658	0.94	1.7690	0.68	−0.0670	0.60
		100	280 962	1.9278	—	−0.0664	—	1.7810	—	−0.0674	—
	0.1	20	186 112	0.2091	18.88	0.0159	42.33	0.2600	14.79	−0.0101	21.84
		40	223 210	0.2542	1.39	0.0154	37.30	0.3026	0.83	−0.0107	17.35
		50	236 736	0.2569	0.33	0.0139	24.06	0.3045	0.20	−0.0114	11.56
		80	265 600	0.2579	0.05	0.0118	4.97	0.3052	0.03	−0.0126	2.50
		90	265 600	0.2578	0.02	0.0115	2.25	0.3053	0.05	−0.0128	1.28
		100	280 962	0.2578	—	0.0112	—	0.3051	—	−0.0129	—

TABLE 2. Effect of domain size on drag and lift coefficients for maximum and minimum separation distances ($l^* = 1.2$ and 9.5) and shear Reynolds number ($Re_\gamma = 10^{-3}$ and 10^{-1}) at $Re_{slip} = 0$. δ is the percentage error in coefficient, relative to results calculated using the largest domain size ($L^* = 100$).

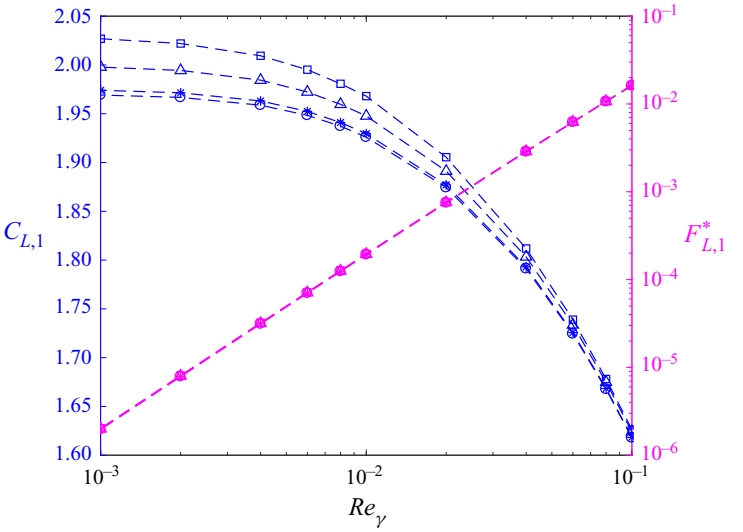

FIGURE 3. Effect of mesh resolution around the sphere on $C_{L,1}$ for a non-rotating particle at $l^* = 1.2$. N_p, N_d = 15 (–□–); 20 (–△–); 25 (–✳–); 30 (–○–).

asymptotes to different finite values as Re_γ approaches zero. A considerable variation of $C_{L,1}$ with mesh refinement is observed, particularly at low Re_γ, however, the relative change in $C_{L,1}$ decreases as N_p and N_d increase. Indeed, increasing N_p and N_d from 25 to 30 only changes $C_{L,1}$ by a small amount, but concurrently increases the total cell count N_t from 158 976 to 310 500, significantly increasing computational memory requirements ($\sim$ 1.2 Tb). Noting that for low Re_γ the force will be negligible anyway, and that across the entire Re_γ range the difference between the $N_p, N_d = 25$ and $N_p, N_d = 30$ results is small anyway, we employed the mesh with $N_p, N_d = 25$ for the remainder of the study.

3. Zero-slip force correlations

In this section, we present results for the lift force (§ 3.2), and then for the drag force (§ 3.3), using the force definitions given in § 3.1.

3.1. *New lift and drag model definitions*

We define the lift force on a particle experiencing both slip and shear within a linear shear flow as

$$F^*_L = C_{L,1} Re^2_\gamma + \mathrm{sgn}(\gamma^*) C_{L,2} Re_\gamma Re_{slip} + C_{L,3} Re^2_{slip}, \tag{3.1a}$$

which may also be written in the alternative form

$$F^*_L = F^*_{L,1} + F^*_{L,2} + F^*_{L,3}. \tag{3.1b}$$

The form chosen for our model is the same as used in the discussed previous inner region studies (Cox & Hsu 1977; Cherukat & McLaughlin 1994), but we now apply this model over the entire inner, outer and unbounded regions. Further, we provide unambiguous definitions for the three coefficients that allow the (3.1) to be a valid representation of the lift force at any separation distance. Namely, the force term $F^*_{L,1} = C_{L,1} Re^2_\gamma$ is defined by the force in a linear shear flow in the absence of slip. The corresponding force coefficient

$C_{L,1}$ (the main focus of this study) depends only on shear rate and wall distance. The last term $F^*_{L,3} = C_{L,3}Re^2_{slip}$ provides the lift in a quiescent flow in the absence of shear, and the force coefficient $C_{L,3}$ is only a function of slip velocity and wall distance. The remaining term $F^*_{L,2} = \mathrm{sgn}(\gamma^*)C_{L,2}Re_\gamma Re_{slip}$ captures the remaining lift contributions in the presence of both slip and shear. Hence, the corresponding force coefficient, $C_{L,2}$ depends upon slip, shear and wall distance.

In the same spirit, the net drag acting on a particle with a finite slip in a linear shear flow, is defined as

$$F^*_D = -\mathrm{sgn}(\gamma)C_{D,1}Re_\gamma - \mathrm{sgn}(u_{slip})C_{D,2}Re_{slip}, \tag{3.2a}$$

which may also be written in the alternative form

$$F^*_D = F^*_{D,1} + F^*_{D,2}. \tag{3.2b}$$

Again, while the form of this equation comes from previous work (Magnaudet *et al.* 2003), our definition of the coefficients ensures that it provides an exact expression for the drag force across all separation distances. Specifically, the force term $F^*_{D,1} = -\mathrm{sgn}(\gamma)C_{L,1}Re_\gamma$ in (3.2) is defined as the drag force in a linear shear flow in the absence of slip. The corresponding force coefficient $C_{D,1}$, valid for all separation distances, is only a function of shear and wall distance. The term $F^*_{D,2} = -\mathrm{sgn}(u_{slip})C_{D,2}Re_{slip}$ in (3.2) captures the remaining drag contributions in the presence of both the slip and shear. The force coefficient $C_{D,2}$, is a function of slip, shear and wall distance.

In the present study, our primary aim is to investigate forces on a particle under zero-slip conditions, and hence provide correlations for the lift and drag force coefficients, $C_{L,1}$ and $C_{D,1}$ respectively. However, in § 4 we do use the full form of (3.1) and (3.2) when applying our new correlations to analyse the movement of force-free particles translating near a wall.

3.2. *Lift force*

In figure 4, lift coefficients $C_{L,1}$ computed for both non-rotating and a freely rotating particles are plotted as a function of separation distance (l^*). The numerical results are compared with the available inner region correlations listed in table 1 that are valid for $Re_\gamma \ll 1$ and $Re_{slip} = 0$. For $Re_\gamma < 10^{-2}$, the numerically computed lift forces in the region close to the wall ($l^* < 2$) agree reasonably well with the asymptotic values predicted by the analytical solutions derived for low Reynolds numbers (Cherukat & McLaughlin 1994; Krishnan & Leighton 1995). Specifically, the lowest shear Reynolds number simulation conducted at the smallest distance to the wall ($l^* = 1.2$) gives a $C_{L,1}$ of 1.993 (1.787) for a non-rotating (freely rotating) particle, which is only ∼1.3 % (5.2 %) higher than the asymptotic value of 1.9680 (1.6988) predicted for a non-rotating (freely rotating) particle at $l^* = 1$ (Krishnan & Leighton 1995). The computed lift coefficients also agree very well with the low Reynolds number theoretical values of 1.9834 (1.7854) for non-rotating (freely rotating) particles at $l^* = 1.2$, as predicted by Cherukat & McLaughlin (1994). However, as illustrated in figure 4(*b*), for a freely rotating particle the Magnaudet *et al.* (2003) lift correlation predicts a larger coefficient of 2.81 at $l^* = 1$ which is inconsistent with the numerical data and the available theories in this region. As explained in Shi & Rzehak (2020), this over-prediction of the lift coefficient near the wall is due to the neglect of the higher-order separation distance terms ($O(1/l^*) > 2$) that are significant when representing lift in the vicinity of the wall. At large l^* the Magnaudet *et al.* (2003) lift correlation gives $C_{L,1} = 1.8$, a result that is consistent with the large l^*

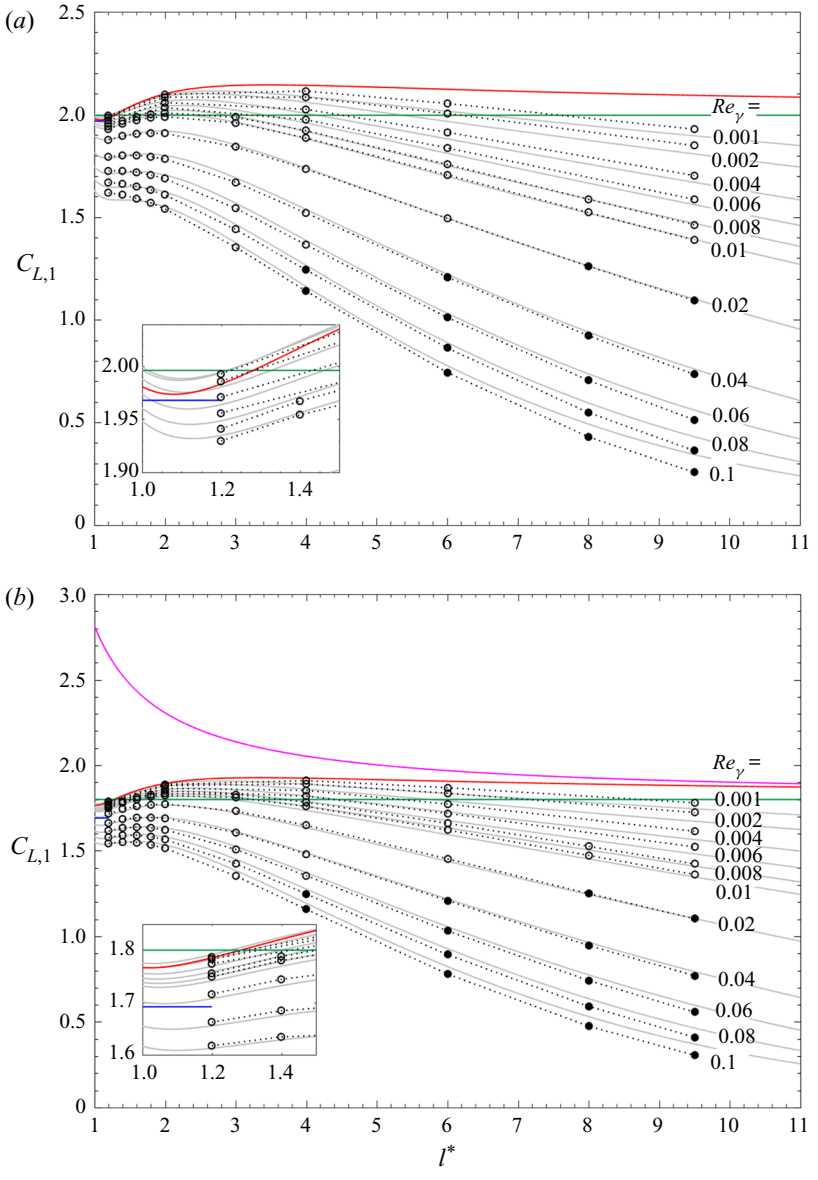

FIGURE 4. Lift coefficient ($C_{L,1}$) for different shear Reynolds number as a function of non-dimensional separation distance (l^*) for (*a*) non-rotating and (*b*) freely rotating spheres. Simulations: inner region (···○···), outer region (···●···). Analytical (1.3), (1.4) (green) from Cox & Hsu (1977), (1.5), (1.6) (red) from Cherukat & McLaughlin (1994), (1.7), (1.8) (blue) from Krishnan & Leighton (1995), (1.9) (pink) from Magnaudet *et al.* (2003). Present numerical fit: (3.3) (grey). Present correlation results for $Re_\gamma = 0$ are coincident with the Cherukat & McLaughlin (1994, 1995) results and not shown on this figure.

value from the Cox & Hsu (1977) lift correlation. However, like all inner region-based models, this large separation limit only has practical relevance for very small Reynolds numbers.

As Re_γ increases and inertial effects become more significant, the computed lift coefficients deviate significantly from the available theoretical values. Even when the

particle is far away from the wall but still within the inner region (e.g. results for $Re_\gamma < 10^{-2}$), the computed lift force coefficient decreases with shear rate, in contrast to the available inner region models which give coefficients that are independent of Re_γ. For example, the Cherukat & McLaughlin (1994) model gives a $C_{L,1}$ of 2.0069 (1.8065) for a non-rotating (freely rotating) particle as $l^* \to \infty$. Eventually, with increasing shear rate and increasing separation distance, the walls move to the outer region ($l^*/{L_G}^* > 1$) and, unsurprisingly, the inner region-based models do not capture the lift coefficient variation well at all. Hence the available inner region-based theoretical lift models overestimate the lift coefficient for all but the lowest shear Reynolds numbers, for particles both near and (especially) further away from the wall.

The discrepancy between simulation and theory arises for the inner region-based models because they use a first-order expansion for the disturbance velocity that cannot satisfy the boundary conditions at infinity (Cherukat & McLaughlin 1994). For many applications relevant to cell sorting in microfluidics, or to understand mechanical phenomena like particle deposition and fouling at $Re_\gamma \lesssim O(1)$, this is problematic, and a single equation for the wall-induced lift force valid across both the inner and outer regions would be beneficial. Therefore, as well as providing a shear-based inertial correction for the analytical inner region model of Cherukat & McLaughlin (1994), we here propose a model that simultaneously captures the outer region behaviour.

In this vein, we first plot the computed lift force coefficients against the separation distance, now normalised using Saffman's length scale (L_G^*). Recall that this length scale defines the boundary between the inner and outer regions in this problem. These results, shown in figure 5, indicate that the outer region data ($l^*/L_G^* > 1$) collapse to a single curve for the selected range of shear Reynolds numbers, similar to the results given for a freely rotating particle at $Re_\gamma \ll 1$ presented by Asmolov (1999). The difference between a non-rotating and freely rotating lift coefficient value is less significant in the outer region, particularly at $l^*/L_G^* \gg 1$. Utilising this outer region behaviour, together with the existing low Re_γ inner region Cherukat & McLaughlin (1994) results, the following lift correlation is proposed for particles moving near a wall under zero-slip conditions:

$$C_{L,1} = f_1(Re_\gamma) C_{outer}(l^*/{L_G}^*) + f_2(Re_\gamma) C_{inner}(1/l^*), \tag{3.3}$$

where

$$f_1(Re_\gamma) = \lambda_1 \exp(\lambda_2 Re_\gamma) + \lambda_3 \exp(\lambda_4 Re_\gamma); \tag{3.4}$$

$$C_{outer}(l^*/L_G^*) = \lambda_5 \exp\left[\lambda_6 \left(l^*/L_G^*\right)^2 + \lambda_7 \left(l^*/L_G^*\right)\right]; \tag{3.5}$$

$$f_2(Re_\gamma) = 1 + \sqrt{Re_\gamma}; \tag{3.6}$$

$$C_{inner}(1/l^*) = \lambda_8 (1/l^*) + \lambda_9 (1/l^*)^2 + \lambda_{10} (1/l^*)^3. \tag{3.7}$$

Coefficients for the above functions are listed in table 3 for both non-rotating and freely rotating particles.

The functions used in (3.3) represent different limits. Within the inner region, the first term of (3.3) rapidly reduces to zero as both $Re_\gamma \to 0$ and $l^* \to 1$, leaving the second part of the equation to be dominant. The function C_{inner} consists of the non-zero degree polynomial terms of the Cherukat & McLaughlin (1994) model. Here, $f_2(Re_\gamma)$, which is independent of wall distance, captures inertial effects when the particle is close to the wall. At $l^* = 1$ and $Re_\gamma = 0$, the product of $f_1(Re_\gamma) C_{outer}$ reduces to the constant value of 2.0069 (1.8065), consistent with the Cherukat & McLaughlin (1994) result for a non-rotating

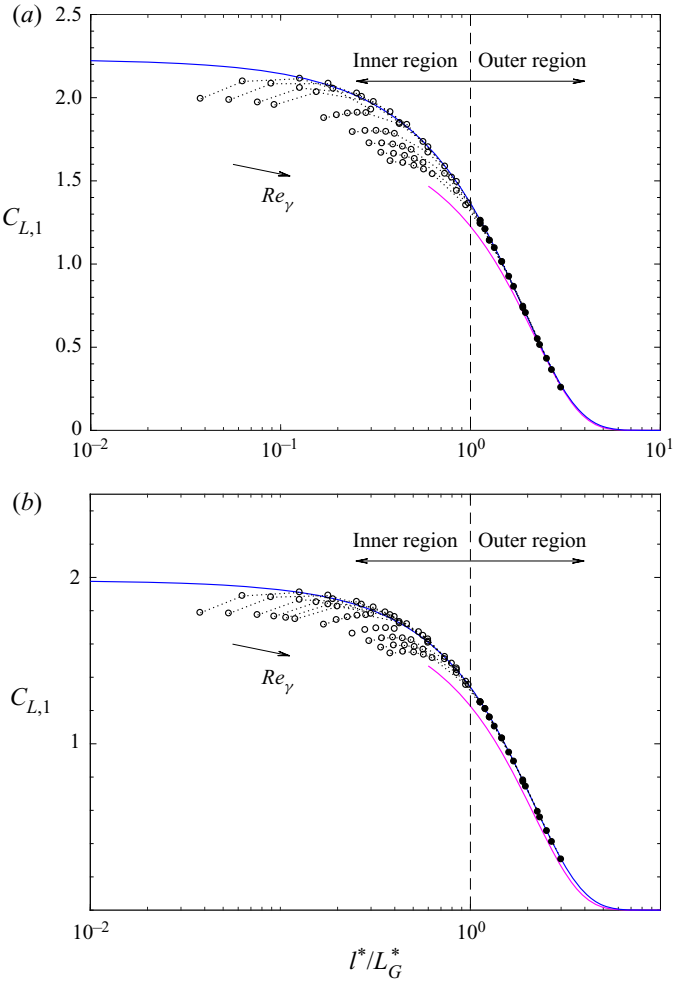

FIGURE 5. Lift coefficient ($C_{L,1}$) for shear Reynolds number values of 1, 2, 4, 6, 8, 10, 20, 40, 60, 80 and 100; $\times 10^{-3}$ (the arrow indicates the direction of increasing Re_γ) as a function of separation distance non-dimensionalised by the Saffman length scale ($l^*/L_G{}^*$) for a (*a*) non-rotating and (*b*) freely rotating particle. Simulations: inner region (···○···), outer region (···●···). Present numerical fit: (3.5) (blue). Asmolov (1999) results for outer region (pink).

(freely rotating) particle. With increasing shear rate and wall distance, the first term of the (3.3) becomes dominant and captures the outer region variation. This term gives zero $C_{L,1}$ as $l^* \to \infty$.

Figure 4 shows that the proposed model captures the simulated lift coefficients accurately over most of the Re_γ range and separation distances considered in this study. For low shear rates ($Re_\gamma \sim 10^{-3}$), the model performs well, slightly underestimating the simulated results with a maximum deviation of 1.6 % (3.2 %) for a non-rotating (freely rotating) particle at distances far from the wall. For high shear rates ($Re_\gamma \sim 10^{-1}$), the model generally overestimates the simulated results, with a maximum deviation of 41 % (21 %) for a non-rotating particle (freely rotating particle) occurring when the particle is furthest from the wall, that is at $l^* = 9.5$. This deviation rapidly reduces down to 4.5 % (5.6 %) for a non-rotating (freely rotating) particle when the separation distance

Coefficient	Non-rotating	Freely rotating
λ_1	0.9300	0.9250
λ_2	−0.8800	−0.3500
λ_3	−0.0300	−0.0135
λ_4	−1000	−7000
λ_5	2.231	1.982
λ_6	−0.1054	−0.1150
λ_7	−0.3859	−0.2771
$\lambda_8{}^a$	1.0575	0.89934
$\lambda_9{}^a$	−2.4007	−1.9610
$\lambda_{10}{}^a$	1.3174	1.0216

TABLE 3. Coefficients for (3.3) for a non-rotating and freely rotating particle.
[a]Coefficients from Cherukat & McLaughlin (1994) and Cherukat & McLaughlin (1995).

decreases to $l^* = 6$, showing that even for the relatively high $Re_\gamma = 10^{-1}$, the proposed model still accurately captures the lift force variation provided that the particle is within a few diameters of the wall. Note that as discussed in § 2.2.1, we expect the numerical data to have the highest errors under the same high Re_γ and l^* conditions that generate the largest deviations between correlation and simulation – conditions that also result in low lift forces. Hence, the proposed model captures the variation of lift coefficient with Re_γ and separation distance reasonably well across all conditions considered, but is most accurate when the resulting lift force is most significant.

3.3. *Drag force*

The drag force on a spherical particle moving parallel to a wall and in the absence of slip is considered in this section. Under these conditions the presence of the wall (combined with the positive shear rate) produces a force on the particle that is in the opposite direction to the flow, and which rapidly decays as the separation distance between the sphere and wall increases. Note that this wall-shear drag causes force-free particles to lag the flow when moving in close proximity to a wall.

Figure 6 shows the variation in drag coefficient $C_{D,1}$ for shear Reynolds numbers in the range $Re_\gamma = 10^{-3}-10^{-1}$ as a function of wall separation distance. Results for both non-rotating and freely rotating conditions are shown.

Figure 6(*a*) is specific to non-rotating particles. The highest drag coefficient magnitudes are observed close to the wall, with a rapid decrease occurring with increasing wall distance or increasing Re_γ. For the largest separation considered ($l^* = 9.5$), small positive $-C_{D,1}$ values of $O(10^{-3})-O(10^{-2})$ are reported for $Re_\gamma = 10^{-1}, 8 \times 10^{-2}$ as illustrated in the inset of figure 6(*a*). As discussed in § 2.2.1, these small positive drag coefficients are more likely to be due to the limited domain size employed in the simulations (numerical accuracy), rather than being physically meaningful.

Figure 6(*b*) shows the drag coefficient for a freely rotating particle as a function of wall distance. The highest negative values for $-C_{D,1}$ are obtained when the particle is close to the wall, reducing to zero with increasing wall distance, in a manner similar to that observed for a non-rotating particle. The highest reported $-C_{D,1}$ values are ∼6 % less than the values reported for a non-rotating particle. The simulated drag coefficient results are also compared with the inner region analytical drag correlation of Magnaudet *et al.* (2003)

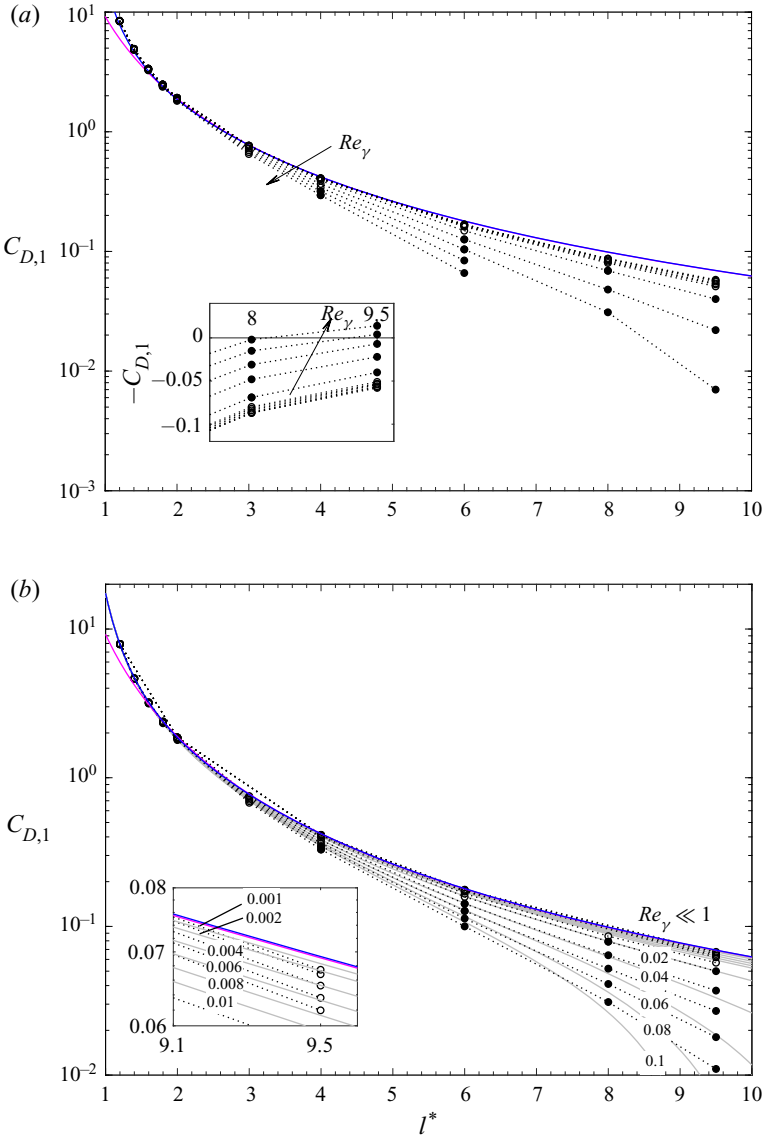

FIGURE 6. Magnitude of drag force coefficient in the absence of slip ($C_{D,1}$) (*a*) for a non-rotating (*b*) freely rotating particle. The arrow indicates the direction of increasing Re_γ. Simulations: inner region (···○···), outer region (···●···). Analytical prediction of Magnaudet *et al.* (2003) (1.11) (pink). Present numerical fits for $Re_\gamma \ll 1$: (3.8) (blue) and finite Re_γ (3.9) (grey).

for a freely rotating particle at low $Re_\gamma \ll 1$. The computed drag coefficients are in good agreement with the correlation values for Reynolds numbers $Re_\gamma < 10^{-2}$ and for wall distances $l^* > 1.6$. However, as the separation distance decreases ($l^* \to 1$), the theoretical predictions of (1.11) underestimate the drag, resulting in a difference of $\sim$32 % at $l^* = 1.2$. This could again be due to the neglect of higher-order terms in the analytical solution, (1.11). In support of this, in the same study by Magnaudet *et al.* (2003), but for zero-shear flows ($Re_\gamma = 0$), the effect of higher-order l^* terms on $C_{D,2}$ was examined in the context

of small separation distances ($l^* < 3$), and it was found that a $\sim 60\,\%$ difference in this drag coefficient occurred when using $O((1/l^*)^3)$ over $O((1/l^*)^5)$ terms in their analysis, for $l^* \to 1$. Similar higher-order terms for the $C_{D,1}$ drag coefficient examined in our study are not available in the literature, however.

The freely rotating drag coefficients shown in figure 6(*b*) also display a dependence on shear rate, as well as separation distance. Generally studies of force-free particles and fixed particles give inertial corrections for $C_{D,1}$ and $C_{D,2}$ in terms of the slip velocity (Re_{slip}) (Kurose & Komori 1999; Magnaudet *et al.* 2003). However, in the present zero-slip context these inertial corrections are not relevant, and instead an inertial correction based on Re_γ is required.

Hence, to accurately predict the variation of $C_{D,1}$ in (3.2) over the shear rates and separation distances considered in this study, we propose a new correlation that is partially based on existing inner region results (Magnaudet *et al.* 2003), but includes two modifications.

Firstly, to capture the drag force variation close to the wall at $Re_\gamma \ll 1$, (1.11) is modified as

$$C'_{D,1} = \frac{15\pi}{8}\left(\frac{1}{l^*}\right)^2\left[1 + \frac{9}{16}\left(\frac{1}{l^*}\right) + 0.5801\left(\frac{1}{l^*}\right)^2 - 3.34\left(\frac{1}{l^*}\right)^3 + 4.15\left(\frac{1}{l^*}\right)^4\right], \tag{3.8}$$

where $C'_{D,1}$ consists of the terms given by Magnaudet *et al.* (2003) in (1.11), combined with three new higher-order terms in separation distance derived through a numerical fitting to our simulation results for $Re_\gamma \ll 1$. The proposed correlation accurately captures the computed drag coefficient down to a minimum separation distance of $l^* = 1.2$. When the particle is in contact with the wall ($l^* = 1$), the current model predicts a finite drag coefficient $-C_{D,1}$ of -17.392 (compared to a value of -9.204 from (1.11)). Whilst the proposed model performs better than the Magnaudet *et al.* (2003) correlation at $l^* = 1.2$, for the limiting case of $l^* = 1$ there is no asymptotic value available for $C_{D,1}$ upon which to validate the new expression.

Secondly, we present an inertial correction to the proposed low Re_γ equation (3.2), based on fits to our data, that predicts the variation of $C_{D,1}$ with finite Re_γ. The final wall-shear drag correlation can be written

$$C_{D,1} = C'_{D,1} + (3.001Re_\gamma^2 - 1.025Re_\gamma), \tag{3.9}$$

where $C'_{D,1}$ is given via (3.8). Although, the new inertial correction accurately captures the shear dependence of $C_{D,1}$ across all considered separations at low Re_γ, far away from the wall ($l^* > 8$) the coefficient is underestimated for $Re_\gamma > 6 \times 10^{-2}$. Note, however, that these are the same conditions that result in the poorest accuracy of the computed $C_{D,1}$, as previously discussed.

4. Application of force correlations

In this section, we analyse the movement of a force-free particle in a linear shear flow using the proposed force correlations. This is accomplished in two parts. First, we use the new drag correlation to find the slip velocity of a particle moving near a wall. Second, this is combined with the new lift correlation to find the lift force acting on the particle and migration velocity of the particle, accounting for both shear and slip effects.

In order to validate these analytical predictions, a small number of additional simulations were performed for force-free (zero-drag) and torque-free particles. For these simulations the net drag acting on the particle in the flow direction $\boldsymbol{F}_p \cdot \boldsymbol{e}_x$ was explicitly set to zero and the slip velocity $\boldsymbol{u}_{slip} \cdot \boldsymbol{e}_x$ in the flow direction was solved as an unknown.

4.1. *Slip velocity*

The slip velocity of a force-free particle is first calculated by setting the net drag force ($F_D{}^*$) in (3.2) to zero. The resulting non-dimensional velocity $u^*_{slip}(= Re_{slip}/Re_\gamma)$ is

$$u^*_{slip} = -\frac{C_{D,1}}{C_{D,2}}. \tag{4.1}$$

The present numerical drag correlation for $C_{D,1}$ provided by (3.9) is used to evaluate the slip velocity for three finite shear Reynolds numbers ($Re_\gamma = 10^{-1}$, 10^{-2}, 10^{-3}) as well as $Re_\gamma = 0$. In these calculations the Faxen drag correlation given by Happel & Brenner (1981) (with higher-order terms up to $O((1/l^*)^5)$) is used to evaluate $C_{D,2}$. Note that this correlation has been derived for the inner region of quiescent flows ($Re_\gamma = 0$) at low slip Reynolds numbers ($Re_{slip} \ll 1$), and yet we are applying it in this section for finite slip Reynolds number in the presence of shear, and across all three regions (inner, outer and unbounded regions). However, although this Faxen drag model is derived for $Re_{slip} \ll 1$, Ambari, Gauthier & Guyon (1984) and Takemura (2004) experimentally showed that this correlation is valid for $Re_{slip} \leq 0.1$ in quiescent flows, partly justifying the use of this correlation for the slip Reynolds numbers considered here. Further, in unbounded linear shear flows, Kurose & Komori (1999) showed that $C_{D,2}$ is nearly independent of shear rate for $Re_{slip} < 5$ and $O(Re_\gamma/Re_{slip}) < 1$. It is also worth mentioning that in quiescent flows, L_S has been used to define the boundary of the inner and outer regions. However, for non-zero-shear flows (as in this case), the inner and outer region boundary is defined based on the $\min(L_S, L_G)$ condition. For this specific case, L_S decays rapidly with separation distance, resulting $L_S \gg L_G$ for all the separation distances and all Re_γ values considered in this study. Hence, L_G is chosen to define the inner and outer regions. However, with respect to L_S (as defined for quiescent flows), the walls are well within the inner region, which may again partly justify the use of $C_{D,2}$ when $L_G < l < L_S$. Hence, while we are applying this $C_{D,2}$ correlation outside its range of validity (i.e. across all three regions and for $Re_\gamma \neq 0$ and $Re_{slip} \neq 0$), evidence suggests that the associated error should not be large.

The calculated u^*_{slip} values are plotted as a function of separation distance in figure 7(*a*). The velocities are compared with: (i) our numerical predictions; (ii) numerical predictions by Fischer & Rosenberger (1987) based on a boundary element method that included small inertial effects ($Re_\gamma \ll 1$); (iii) theoretical/numerical predictions by Goldman *et al.* (1967*b*) applicable to Stokes flow; (iv) slip velocities again calculated using (4.1), but with $C_{D,1}$ evaluated using the Magnaudet *et al.* (2003) correlation of (1.11).

Consistent with earlier studies (Goldman *et al.* 1967*b*; Takemura & Magnaudet 2009), the negative slip velocities obtained confirm that a force-free particle translating in a linear shear flow lags the fluid when in close proximity to a wall. The present correlation, (3.9), used for evaluating $C_{D,1}$ predicts a slip velocity that is consistent with the all available numerical results down to reasonably small separation distances ($l^* \sim 1.1$). In comparison the results obtained using the Magnaudet *et al.* (2003) correlation ((1.11)) diverge from the numerical results at $l^* \sim 1.5$. At small separation distances ($l^* \lesssim 1.1$) the two numerical results diverge. The predicted Stokes flow velocities from Goldman *et al.* (1967*b*) exhibit large negative values when the particle is almost in contact with the wall ($l^* \sim 1$), whereas

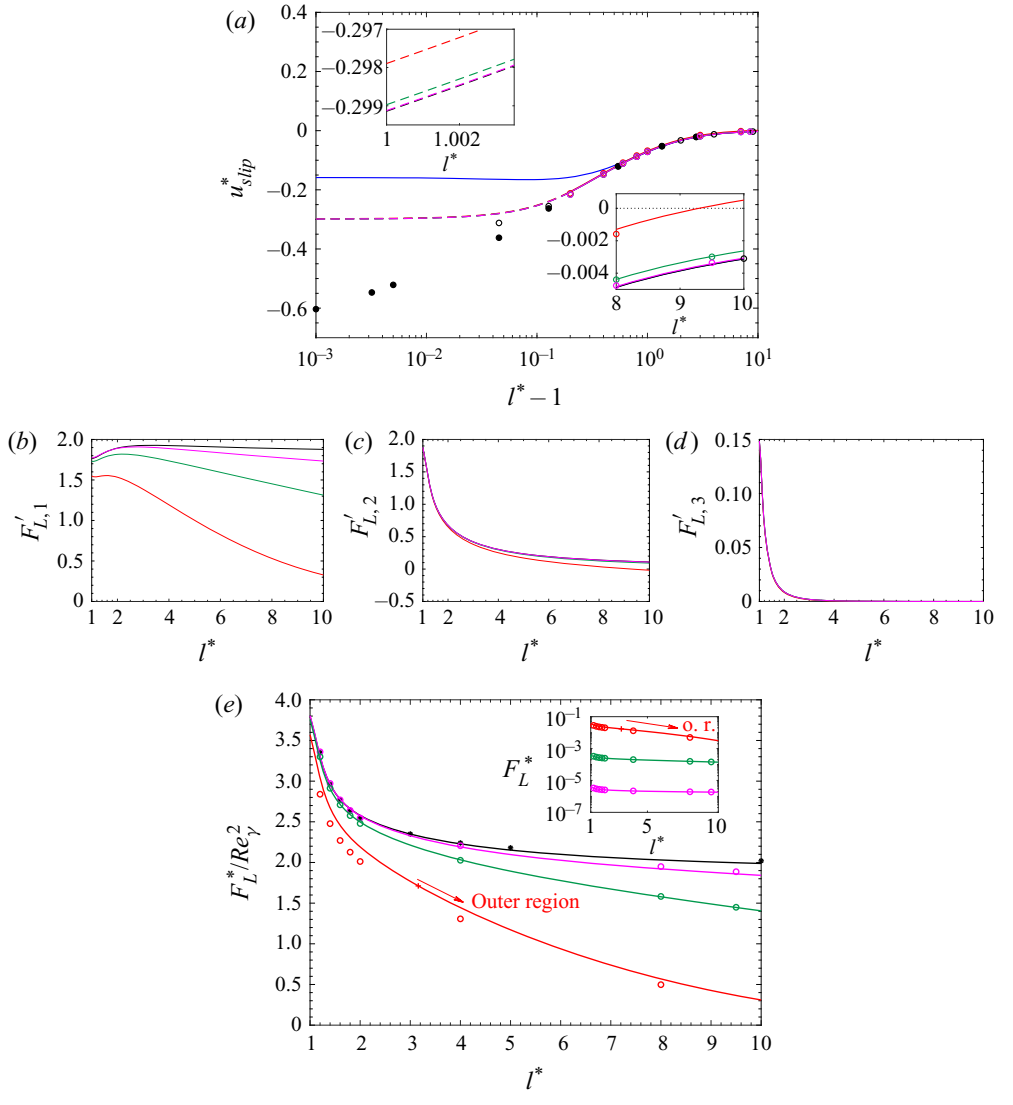

FIGURE 7. Analysis of a force-free particle translating in a linear shear flow near a wall. (*a*) Non-dimensional slip velocity when $C_{D,1}$ is evaluated using the present numerical correlation, (3.9) for $Re_\gamma = 0$ (black), $Re_\gamma = 10^{-3}$ (pink), $Re_\gamma = 10^{-2}$ (green), $Re_\gamma = 10^{-1}$ (red). Dashed lines indicate results evaluated outside the strict range in which the new correlation has been validated. Slip velocity when $C_{D,1}$ is evaluated using the Magnaudet *et al.* (2003) correlation, (1.11) for $Re_\gamma = 0$ (blue); Fischer & Rosenberger (1987) numerical results for $Re_\gamma \ll 1$ (○); Goldman *et al.* (1967*b*) numerical results for Stokes flow (●); present force-free numerical results (coloured hollow circles). (*b–d*) Different contributions to the net lift force acting on the particle, $F'_{L,1}$, $F'_{L,2}$ and $F'_{L,3}$ representing shear, slip-shear and slip effects, respectively. (*e*) Net lift force non-dimensionalised by shear Reynolds number when $F'_{L,tot}$ is evaluated using (4.3) for $Re_\gamma = 0$ (black), $Re_\gamma = 10^{-3}$ (pink), $Re_\gamma = 10^{-2}$ (green), $Re_\gamma = 10^{-1}$ (red); Fischer & Rosenberger (1987) numerical results for $Re_\gamma \ll 1$ (∗); present force-free numerical results (coloured hollow circles).

the few results of Fischer & Rosenberger (1987) in this region, that are valid for small but finite inertial effects, show smaller slip velocities. The difference between Fischer & Rosenberger (1987) and Goldman *et al.* (1967*b*) may be due to insufficient numerical accuracy of a Gauss–Legendre product formula used by Fischer & Rosenberger (1987), as suggested by Shi & Rzehak (2020). We make no further comment on this difference, but note that the extrapolation of our correlation (indicted by the dashed lines in figure 7*a*) appears to be more consistent with the Fischer & Rosenberger (1987) results at $l^* = 1.05$ than those of Goldman *et al.* (1967*b*).

Slip velocity curves for the selected range of Reynolds numbers suggest that the shear rate has only a small effect ($\sim O(10^{-3})$) on u^*_{slip} for all separation distances. As expected, predicted slip velocities reduce to small values with increasing separation distance for the low $Re_\gamma = 10^{-3}, 10^{-2}$ cases. However, for $Re_\gamma = 10^{-1}$ the effect of inertia is relatively more important and the slip velocity further reduces, becoming approximately zero. In fact, small positive slip velocities are predicted under the conditions $Re_\gamma = 10^{-1}$ and $l^* > 9.2$. However, as mentioned in § 3.3, numerical inaccuracy of the fitted correlation, (3.9), at large separation distances for high Re_γ, is more likely to be the main reason that such positive slip velocities are obtained, rather than being physically meaningful. Significantly, the slip velocities are very small in this high separation distance region for all Re_γ considered.

4.2. *Lift force and migration velocity*

By using the slip velocity calculated via (4.1) and the lift formulation given in (3.1), the lift force on a force-free particle experiencing both slip and shear within a linear shear flow can be written

$$\frac{F^*_L}{Re^2_\gamma} = C_{L,1} + C_{L,2}u^*_{slip} + C_{L,3}{u^*_{slip}}^2, \tag{4.2}$$

which may also be written in the alternative form

$$F'_{L,tot} = F'_{L,1} + F'_{L,2} + F'_{L,3}. \tag{4.3}$$

Again, note that the form of (4.3) is valid for all three regions (inner, outer, unbounded), provided that the lift coefficients used are valid in all three regions. Here, however, lift force coefficients for $C_{L,2}$ and $C_{L,3}$ are evaluated using the Cherukat & McLaughlin (1995) inner region-based correlations as there are no correlations available for these coefficients which span all three regions. $C_{L,1}$ is evaluated using our freely rotating particle correlation, as given by (3.3), which is valid across all three regions. Here $F'_{L,tot}(= F^*_L/Re^2_\gamma)$ is the net lift force non-dimensionalised by shear Reynolds number.

The lift contributions, as well as the net lift force, are plotted in figure 7 for $Re_\gamma \ll 1$ and $Re_\gamma = 10^{-3}, 10^{-2}, 10^{-1}$. The numerical lift results obtained from our force-free and torque-free particles simulations are also given in figure 7(*e*). For separation distances $l^* \gtrsim 2$, the force contributions illustrate that $F'_{L,1} > F'_{L,2} \gg F'_{L,3}$ for a force-free particle. This indicates that the wall-shear lift contribution, $C_{L,1}$, either dominates or is similar to the other forces in this high force region, with the consequence that an accurate inertial correction for $C_{L,1}$ is required to accurately predict the net lift force acting on a force-free particle. Figure 7(*e*) also shows that the estimated $F'_{L,tot}$ using our correlations agrees well with the low Re_γ results of Fischer & Rosenberger (1987) (using $Re_\gamma = 0$ in our correlation), but deviates significantly from these results as the shear Reynolds number and separation distance increase. Most of our numerical results agree reasonably well with (4.3) predictions for the selected separation distances and shear Reynolds number ranges.

The present numerical results clearly exhibit the inertial dependence predicted by new lift model, and thus reinforces the importance of the Reynolds number correction to $C_{L,1}$.

Interestingly, the inset of figure 7(*e*) illustrates that the net lift force, F_L^*, while increasing with shear rate, is relatively independent of separation distance, except at the highest Re_γ considered. When Re_γ is low, the net lift (and the lift coefficient) does not reduce to zero until well into the outer region, which for low Re_γ is a large distance from the wall: for $Re_\gamma = 10^{-2}$ and 10^{-3}, the transition from the inner to the outer region (L_G^*) occurs at $l^* = 10$ and 31.62, respectively. Therefore, a clear lift dependence on the separation distance is not visible in figure 7(*e*) as the maximum l^* indicated is 10. Nevertheless, a strong lift dependence on the separation distance is visible for the largest particle shear Reynolds number ($Re_\gamma = 10^{-1}$) as the transition from the inner to outer region occurs at $l^* = 3.16$, well within the region of analysis.

The minor deviations between numerical and correlation results observed in the predicted lift force for the highest Re_γ could be a result of two factors. Firstly, as discussed in § 3.2, at high Re_γ our freely rotating $C_{L,1}$ correlation slightly overestimates the lift force, particularly far from the wall. Secondly, there are errors in using the inner region-based correlations for $C_{L,2}$ and $C_{L,3}$ in our analysis. The main draw back is the overestimation of the slip-based lift forces when the particle is far from the wall. This happens as a result of $C_{L,2}$ and $C_{L,3}$ reducing to the outer boundary values of the inner region, instead of reducing to the unbounded values as $l^* \to \infty$. Additionally, the inertial dependence of $F'_{L,2}$ and $F'_{L,3}$ is weakly captured with the current coupling, as the inner region models for $C_{L,2}$ and $C_{L,3}$ are derived for $Re_\gamma, Re_{slip} \ll 1$ and $Re_{slip} \ll 1$ conditions, respectively. However, for the present case of a force-free particle, these two limitations are not that significant because u^*_{slip} rapidly reduces with increasing l^* (figure 7*a*). Therefore the slip-based lift forces, $F'_{L,2}$ and $F'_{L,3}$ contribute only a small amount to the overall lift force for $l^* > 2$. Whenever slip becomes significant for the case of a force-free particle, the walls are well within the inner region ($l^* < 2$), and therefore the net lift correlation reduces to the original Cherukat & McLaughlin (1995) inner region correlation. However, for relatively large slip velocities (e.g. buoyant particles near walls), where $F'_{L,2}$ and $F'_{L,3}$ are more significant, predictions of (4.3) with inner region-based slip lift coefficients will be not necessarily be accurate. This is a limitation which needs to be addressed in future studies in order to completely generalise the net lift model given by (3.1).

Dimensionless migration velocities $u^*_{mig} (= u_{mig}/\gamma a)$ obtained by balancing the lift force and the wall-normal drag force,

$$u^*_{mig} = \frac{F_L^*}{6\pi Re_\gamma (1 + C_{D\perp})} \tag{4.4}$$

are presented in figure 8(*a*) for the same set of shear Reynolds numbers. Here, $C_{D\perp}$, the wall-bounded drag coefficient of a particle translating normal to a wall, is evaluated via the analytical inner region correlation of Faxen (1922) and Happel & Brenner (1981). The migration velocities obtained by balancing the lift with Stokes unbounded drag ($C_{D\perp} = 0$ in (4.4)) are also shown in the same figure using dashed lines. It is evident that the wall-normal correction to the Stokes drag greatly decreases the migration velocity close to the wall. Noting that $C_{D\perp}$ is an inner region model which rapidly decays to zero we assume that $C_{D\perp}$ can be used for all the separation distances to predict the migration velocity of a particle. Based on the migration velocity normal to the wall and the particle velocity parallel to the wall, we can calculate the lateral displacement in the wall-normal direction (h) and longitudinal displacement in the flow direction (d)

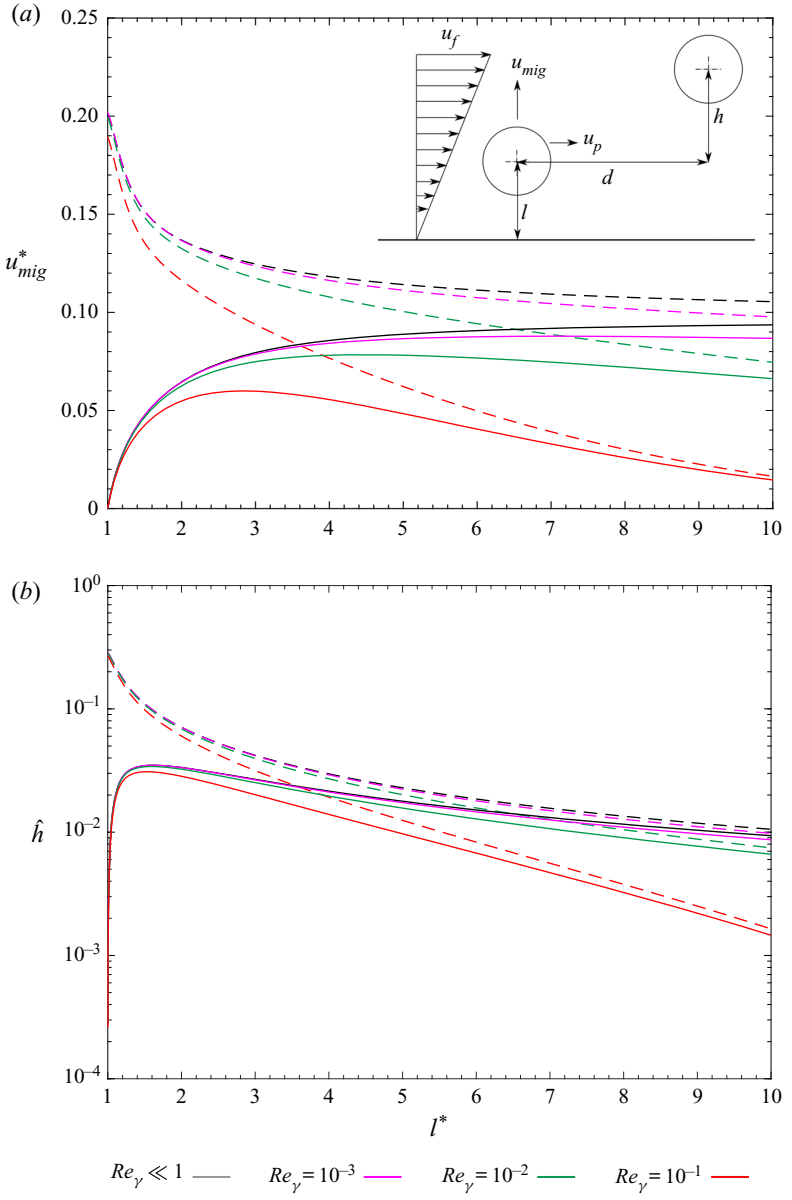

FIGURE 8. (*a*) Dimensionless migration velocity and (*b*) Lateral displacement per unit movement in the flow direction of a force-free particle for $Re_\gamma \ll 1$, $Re_\gamma = 10^{-3}$, $Re_\gamma = 10^{-2}$ and $Re_\gamma = 10^{-1}$. Dashed lines show the values obtained when $C_{D\perp} = 0$ in (4.4). Here, $\hat{h} = h/d$, $l^* = l/a$ and $u^*_{mig} = u_{mig}/\gamma a$.

as illustrated in figure 8(*a*). The calculated lateral displacement per unit longitudinal displacement $\hat{h}(= h/d)$ of a particle located at l^* is also given in figure 8(*b*). For all shear Reynolds numbers the lateral displacement of a force-free particle closer to the wall is much higher than that of a particle travelling further away from the wall. The maximum lateral displacement $\hat{h} \sim 0.035$ that occurs when the particle is closer to the wall ($l^* \sim 1.5$)

would quite quickly push a free particle away from the wall. The lateral displacement also displays a weak dependence on the shear rate close to the wall ($l^* \sim 1$), however, when a particle is away from the wall $\hat{h}$ decreases significantly as the shear Reynolds number increases.

Although the present study focuses on linear shear flows, it is interesting to briefly discuss the behaviour of lift coefficients of force-free particles in Poiseuille flows at $Re_\gamma < 1$. Direct numerical studies on planar Poiseuille flows have shown that the net lift coefficient ($F'_{L,tot}$) of force-free particles is relatively independent of Re_γ even when $Re_\gamma \sim O(10^{-1})$ (Hood, Lee & Roper 2015; Asmolov *et al.* 2018). This discrepancy is possibly due to the weak inertial dependency of the double wall-bounded shear gradient lift force (Schonberg & Hinch 1989; Asmolov 1999) which is not relevant for linear flows. However, as shown in the present linear shear flow study which has a uniform local Re_γ throughout the separation distance, the net lift is clearly dependent on Re_γ, particularly away from the wall.

5. Conclusion

The lift and drag forces acting on a spherical particle in a single wall-bounded linear shear flow field are examined via numerical computation. Forces are obtained under a zero-slip condition, by setting the particle to translate at the same velocity as fluid. The Navier–Stokes equations are solved using a finite volume solver to find the fluid flow around the particle. The effect of shear rate and wall presence are investigated by varying the shear Reynolds number over the range $Re_\gamma = 10^{-3}{-}10^{-1}$, and the wall separation distance over $l^* = 1.2{-}9.5$. Sensitivity analyses show that large computational flow domains, combined with careful mesh construction, are required to accurately predict these forces at these low shear rates and wall separations. Computed lift and drag coefficients at $Re_\gamma \sim O(1)$ are compared against theoretical values, predicted by asymptotic models mainly derived for $Re_\gamma \ll 1$. Accounting for the variations, slip independent inertial corrections are suggested for both the lift and drag force coefficients.

The computed lift force coefficients at the lowest Reynolds numbers are in good agreement with the previous theoretical results when the particle is close to the wall (Cox & Hsu 1977; Cherukat & McLaughlin 1994; Krishnan & Leighton 1995). With increasing shear rate, a significant decrease of the computed lift coefficient is observed for both non-rotating and freely rotating particles. This decrease of lift coefficient is further enhanced when the wall is away from the particle and is located in the outer region. Numerical lift correlations for non-rotating and freely rotating conditions are presented, accounting for both the inner and outer region behaviour in the limit of finite (Re_γ). These expressions reduce to theoretical values predicted in the three limits of $Re \to 0$, $l^* \to 1$ and $l^* \to \infty$.

Drag force coefficients computed for the freely rotating sphere agree reasonably well with low (Re_γ) results from a previous analytical study over most of the wall separation range (Magnaudet *et al.* 2003), however, considerable deviation is seen when the particle is within one radius of the wall. Consequently a drag coefficient model is proposed that includes higher-order terms in separation distance (up to $O((1/l^*)^6)$) that more accurately captures this near-wall drag behaviour. A shear-based inertial correction, independent of slip velocity, is also provided for the modified drag coefficient.

The behaviour of a force-free particle suspended in a linear shear flow is analysed using the new drag and lift correlations. Slip velocities calculated within the range of

validity of our correlations compare favourably with previously presented results that are valid for low (Re_γ). The negative slip velocities indicate that force-free particles lag the fluid near walls for low (Re_γ). Noting the limitations associated with existing slip-based lift coefficients, the lift force on a force-free particle at finite (Re_γ), accounting for both shear-induced slip and slip-induced lift, is also analysed. A rapid decrease of the lift force is observed as both the shear Reynolds number and separation distance increase. This behaviour is not captured via existing analytical lift correlations that are limited to $Re \ll 1$. Interestingly, a maximum lateral displacement per distance travelled of $\sim$0.035 occurs when the particle is separated from the wall by approximately half its radius.

Overall, the suggested zero-slip correlations will aid in providing accurate constitutive equations for interphase forces to predict the behaviour of particles moving near walls.

Acknowledgements

Support from the Australian Research Council (LP160100786) and CSL is gratefully acknowledged. One of the authors (N.E.) acknowledges the support from the Melbourne Research Scholarships program of The Melbourne University. The authors thank the reviewers for their insightful comments.

Declaration of interests

The authors report no conflict of interest.

Appendix

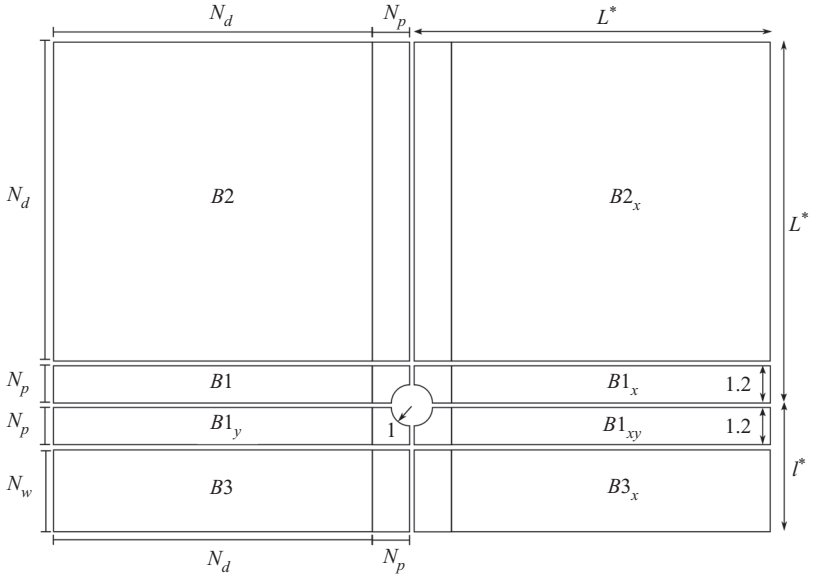

FIGURE 9. A detailed two-dimensional frame at $z = 0$ of a 'Lego' mesh showing how individual blocks are duplicated to form the complete mesh. N_d, N_p and N_w indicate number of points, while L^*, l^* are dimensionless domain sizes.

REFERENCES

AMBARI, A., GAUTHIER, M. B. & GUYON, E. A. 1984 Wall effects on a sphere translating at constant velocity. *J. Fluid Mech.* **149** (1), 235–253.

ASMOLOV, E. S. 1989 Lift force exerted on a spherical particle in a laminar boundary layer. *Fluid Dyn.* **24** (5), 710–714.

ASMOLOV, E. S. 1990 Dynamics of a spherical particle in a laminar boundary layer. *Fluid Dyn.* **25** (6), 886–890.

ASMOLOV, E. S. 1999 The inertial lift on a spherical particle in a plane poiseuille flow at large channel Reynolds number. *J. Fluid Mech.* **381**, 63.

ASMOLOV, E. S., DUBOV, A. L., NIZKAYA, T. V., HARTING, J. & VINOGRADOVA, O. I. 2018 Inertial focusing of finite-size particles in microchannels. *J. Fluid Mech.* **840**, 613–630.

BATCHELOR, G. K. 1967 *An Introduction to Fluid Dynamics*. Cambridge University Press.

BIRD, R. B., STEWART, W. E. & LIGHTFOOT, E. N. 2002 *Transport Phenomena*, 2nd edn. John Wiley & Sons.

BRETHERTON, F. P. 1962 The motion of rigid particles in a shear flow at low Reynolds number. *J. Fluid Mech.* **14** (2), 284–304.

CHERUKAT, P. & MCLAUGHLIN, J. B. 1994 The inertial lift on a rigid sphere in a linear shear flow field near a flat wall. *J. Fluid Mech.* **263** (1), 1–18.

CHERUKAT, P. & MCLAUGHLIN, J. B. 1995 The inertial lift on a rigid sphere in a linear shear flow field near a flat wall. *J. Fluid Mech.* **285**, 407.

COX, R. G. & BRENNER, H. 1968 The lateral migration of solid particles in poiseuille flow – I theory. *Chem. Engng Sci.* **23** (2), 147–173.

COX, R. G. & HSU, S. K. 1977 The lateral migration of solid particles in a laminar flow near a plane. *Intl J. Multiphase Flow* **3** (3), 201–222.

DANDY, D. S. & DWYER, H. A. 1990 A sphere in shear flow at finite Reynolds number: effect of shear on particle lift, drag, and heat transfer. *J. Fluid Mech.* **216**, 381–410.

DI CARLO, D., EDD, J. F., HUMPHRY, K. J., STONE, H. A. & TONER, M. 2009 Particle segregation and dynamics in confined flows. *Phys. Rev. Lett.* **102** (9), 094503.

DREW, D. A. 1988 The lift force on a small sphere in the presence of a wall. *Chem. Engng Sci.* **43** (4), 769–773.

EKANAYAKE, N. I., BERRY, J. D., STICKLAND, A. D., MUIR, I. L., DOWER, S. K. & HARVIE, D. J. 2018 Lift and drag forces on a particle near a wall at low Reynolds numbers. In *21st Australasian Fluid Mechanics Conference, Adelaide, Australia*.

FAXEN, H. 1922 Der widerstand gegen die bewegung einer starren kugel in einer zähen flüssigkeit, die zwischen zwei parallelen ebenen wänden eingeschlossen ist. *Ann. Phys.* **373** (10), 89–119.

FISCHER, T. M. & ROSENBERGER, R. 1987 A boundary integral method for the numerical computation of the forces exerted on a sphere in viscous incompressible flows near a plane wall. *Z. Angew. Math. Phys.* **38** (3), 339–365.

GEUZAINE, C. & REMACLE, J. 2009 Gmsh: A 3-D finite element mesh generator with built-in pre- nd post-processing facilities. *Intl J. Numer. Meth. Engng* **79** (11), 1309–1331.

GOLDMAN, A. J., COX, R. G. & BRENNER, H. 1967*a* Slow viscous motion of a sphere parallel to a plane wall—I motion through a quiescent fluid. *Chem. Engng Sci.* **22** (4), 637–651.

GOLDMAN, A. J., COX, R. G. & BRENNER, H. 1967*b* Slow viscous motion of a sphere parallel to a plane wall—II. Couette flow. *Chem. Engng Sci.* **22** (4), 653–660.

HALOW, J. S. & WILLS, G. B. 1970 Experimental observations of sphere migration in Couette systems. *Ind. Engng Chem. Fundam.* **9** (4), 603–607.

HAPPEL, J. & BRENNER, H. 1981 *Low Reynolds Number Hydrodynamics. [Electronic Resource]: With Special Applications to Particulate Media*. Springer.

HARVIE, D. J. E. 2010 An implicit finite volume method for arbitrary transport equations. *ANZIAM J.* **52**, C1126.

HO, B. P. & LEAL, L. G. 1974 Inertial migration of rigid spheres in two-dimensional unidirectional flows. *J. Fluid Mech.* **65** (02), 365.

HOOD, K., LEE, S. & ROPER, M. 2015 Inertial migration of a rigid sphere in three-dimensional poiseuille flow. *J. Fluid Mech.* **765**, 452–479.

KRISHNAN, G. & LEIGHTON, D. 1995 Inertial lift on a moving sphere in contact with a plane wall in a shear flow. *Phys. Fluids* **7** (11), 2538–2545.

KUROSE, R. & KOMORI, S. 1999 Drag and lift forces on a rotating sphere in a linear shear flow. *J. Fluid Mech.* **384**, 183–206.

LEE, H. & BALACHANDAR, S. 2010 Drag and lift forces on a spherical particle moving on a wall in a shear flow at finite Re. *J. Fluid Mech.* **657**, 89–125.

LEIDERMAN, K. & FOGELSON, A. L. 2011 Grow with the flow: a spatial-temporal model of platelet deposition and blood coagulation under flow. *Math. Med. Biol.* **28** (1), 47–84.

LEIGHTON, D. & ACRIVOS, A. 1985 The lift on a small sphere touching a plane in the presence of a simple shear flow. *Z. Angew. Math. Phys.* **36** (1), 174–178.

MAGNAUDET, J., TAKAGI, S. H. U. & LEGENDRE, D. 2003 Drag, deformation and lateral migration of a buoyant drop moving near a wall. *J. Fluid Mech.* **476**, 115–154.

MCLAUGHLIN, J. B. 1991 Inertial migration of a small sphere in linear shear flows. *J. Fluid Mech.* **224**, 261–274.

MCLAUGHLIN, J. B. 1993 The lift on a small sphere in wall-bounded linear shear flows. *J. Fluid Mech.* **246**, 249–265.

RUBINOW, S. I. & KELLER, J. B. 1961 The transverse force on a spinning sphere moving in a viscous fluid. *J. Fluid Mech.* **11** (3), 447–459.

SAFFMAN, P. G. T. 1965 The lift on a small sphere in a slow shear flow. *J. Fluid Mech.* **22** (02), 385–400.

SCHONBERG, J. A. & HINCH, E. J. 1989 Inertial migration of a sphere in poiseuille flow. *J. Fluid Mech.* **203**, 517–524.

SEGRE, G. & SILBERBERG, A. 1962 Behaviour of macroscopic rigid spheres in poiseuille flow. Part 2. Experimental results and interpretation. *J. Fluid Mech.* **14** (1), 136–157.

SHI, P. & RZEHAK, R. 2020 Lift forces on solid spherical particles in wall-bounded flows. *Chem. Engng Sci.* **211**, 115264.

TAKEMURA, F. 2004 Migration velocities of spherical solid particles near a vertical wall for Reynolds number from 0.1 to 5. *Phys. Fluids* **16** (1), 204.

TAKEMURA, F. & MAGNAUDET, J. 2003 The transverse force on clean and contaminated bubbles rising near a vertical wall at moderate Reynolds number. *J. Fluid Mech.* **495**, 235–253.

TAKEMURA, F. & MAGNAUDET, J. 2009 Lateral migration of a small spherical buoyant particle in a wall-bounded linear shear flow. *Phys. Fluids* **21** (8), 083303.

TAKEMURA, F., MAGNAUDET, J. & DIMITRAKOPOULOS, P. 2009 Migration and deformation of bubbles rising in a wall-bounded shear flow at finite Reynolds number. *J. Fluid Mech.* **634**, 463–486.

VASSEUR, P. & COX, R. G. 1976 The lateral migration of a spherical particle in two-dimensional shear flows. *J. Fluid Mech.* **78** (02), 385.

VASSEUR, P. & COX, R. G. 1977 The lateral migration of spherical particles sedimenting in a stagnant bounded fluid. *J. Fluid Mech.* **80** (3), 561–591.

ZENG, L., BALACHANDAR, S. & FISCHER, P. 2005 Wall-induced forces on a rigid sphere at finite Reynolds number. *J. Fluid Mech.* **536** (1), 1.

ZENG, L., FADY, N., BALACHANDAR, S. & FISCHER, P. 2009 Forces on a finite-sized particle located close to a wall in a linear shear flow. *Phys. Fluids* **21** (3), 033302.